



Magmatic-Hydrothermal Processes of Vein-Type Haman-Gunbuk-Daejang Copper Deposits in the Gyeongnam Metallogenic Belt in South Korea

Tong Ha Lee¹, Jung Hun Seo^{1*}, Bong Chul Yoo², Bum Han Lee², Seung Hee Han³, Yun Seok Yang^{1,3} and Jun Hee Lee¹

¹Department of Energy Resources and Engineering, Inha University, Incheon, South Korea, ²Convergence Research Center for Development of Mineral Resources (DMR), Korea Institute of Geosciences and Mineral Resources, Daejeon, South Korea, ³Korea Polar Research Institute, Incheon, South Korea

OPEN ACCESS

Edited by:

Jung-Woo Park,
Seoul National University, South Korea

Reviewed by:

Khin Zaw,
University of Tasmania, Australia

Pei Ni,
Nanjing University, China

*Correspondence:

Jung Hun Seo
seo@inha.ac.kr

Specialty section:

This article was submitted to
Economic Geology,
a section of the journal
Frontiers in Earth Science

Received: 03 August 2021

Accepted: 08 November 2021

Published: 24 November 2021

Citation:

Lee TH, Seo JH, Yoo BC, Lee BH, Han SH, Yang YS and Lee JH (2021) Magmatic-Hydrothermal Processes of Vein-Type Haman-Gunbuk-Daejang Copper Deposits in the Gyeongnam Metallogenic Belt in South Korea. *Front. Earth Sci.* 9:752908. doi: 10.3389/feart.2021.752908

Haman, Gunbuk, and Daejang deposits are neighboring vein-type hydrothermal Cu deposits located in the SE part of the Korean Peninsula. These three deposits are formed by magmatic-hydrothermal activity associated with a series of Cretaceous granodioritic intrusions of the Jindong Granitoids, which have created a series of veins and alterations in a hornfelsed shale formation. The copper deposits have common veining and alteration features: 1) a pervasive chlorite-epidote alteration, cut by 2) Cu-Pb-Zn-bearing quartz veins with a tourmaline-biotite alteration, and 3) the latest barren calcite veins. Chalcopyrite, pyrite, and pyrrhotite are common ore minerals in the three deposits. Whereas magnetite is a dominant mineral in the Haman and Gunbuk deposits, no magnetite is present, but sphalerite and galena are abundant in the Daejang deposit. Ore-bearing quartz veins have three types of fluid inclusions: 1) liquid-rich, 2) vapor-rich, and 3) brine inclusions. Hydrothermal temperatures obtained from the brine inclusion assemblages are about 340–600, 250–500, and 320–460°C in the Haman, Gunbuk, and Daejang deposits, respectively. The maximum temperatures (from 460 to 600°C) recorded in the fluid inclusions of the three deposits are higher than those of the Cu ore precipitating temperature of typical porphyry-like deposits (from 300 to 400°C). Raman spectroscopy of vapor inclusions showed the presence of CO₂ and CH₄ in the three deposits, which indicates relatively reduced hydrothermal conditions as compared with typical porphyry deposits. The Rb/Sr ratios and Cs concentrations of brine inclusions suggest that the Daejang deposit was formed by a later and more fractionated magma than the Haman and Gunbuk deposits, and the Daejang deposit has lower Fe/Mn ratios in brine inclusions than the Haman and Gunbuk deposits, which indicates contrasting redox conditions in hydrothermal fluids possibly caused by an interaction with a hosting shale formation. In brines, concentrations of base metals do not change significantly with temperature, which suggests that significant ore mineralization precipitation is unlikely below current exposure levels, especially at the Haman deposit. Ore and alteration mineral petrography and fluid inclusions suggest that the Haman deposit was formed near the top of the deep intrusion center, whereas the Gunbuk deposit was formed at a

shallower intrusion periphery. The Daejang deposit was formed later at a shallow depth by relatively fractionated magma.

Keywords: haman, gunbuk, daejang, gyeongnam metallogenic belt, hydrothermal alteration, fluid inclusions, LA-ICP-MS

INTRODUCTION

The Haman, Gunbuk, and Daejang deposits occur within the Gyeongnam belt in the southeastern part of the Korean Peninsula, which is a Cu-bearing province in South Korea, and the area has been well investigated for Cu ores (Sillitoe, 1980; Jin et al., 1982; Lee et al., 2003). The Gyeongnam belt hosts numerous hydrothermal vein- and breccia-type copper deposits (Koh et al., 2003; Choi et al., 2006) associated with a porphyritic granodiorite-granite-quartz monzonite resulting from late Cretaceous igneous activities (Bulguksa orogeny: 115–70 Ma) (Min et al., 1982). The Haman, Gunbuk, and Daejang deposits are vein-type Cu deposits in the Gyeongnam metallogenic belt (Choi, 1985; Shin et al., 1987) and are geographically neighboring and hosted in a Cretaceous shale formation (Haman-Jindong shale formations) and Cretaceous granitoids (Jindong Granitoids) (Park et al., 1985; Shin et al., 1987). These three deposits have been studied intensively because the area is regarded to have potential porphyry-style Cu mineralization (Choi, 1985; Park et al., 1985). The Haman and Gunbuk deposits consist of eight orebodies with an ore grade of 1–6 Cu wt% and a tonnage of 1,450 kt (Kim, 1973). The Daejang deposit is located NW of the Haman and Gunbuk deposits and consists of two orebodies and prospects. The ore grades and tonnages of the Daejang deposit have not been reported.

Numerous geologic and geochemical studies have been conducted on the ore deposits in the Haman, Gunbuk, and Daejang deposit areas. Park et al. (1985) reported high metal contents (e.g. Cu, Zn, and Pb) in the Jindong Granitoids as compared with other nearby Cretaceous granitoids. The wide range of salinities (6–68 wt% NaCl equiv.) determined for ore-mineralized fluids in the Haman and Gunbuk deposits (Park et al., 1985) was suggested to have been caused by hydrothermal system changes from an early lithostatic-magmatic fluid into a later meteoric-dominated hydrostatic fluid system (Choi, 1985). Such a hydrothermal evolution in the area was supported by oxygen and hydrogen isotope analysis (Heo et al., 2003). In the Daejang deposit, Shin et al. (1987) presented a range of pressures up to 4.0 kb, which was estimated by FeS analysis on sphalerite, and temperatures of 250–430°C based on AsS analysis on arsenopyrite. Park and Kim (1988) subdivided mineralizations in the Daejang deposit into stages; 1) the earliest base-metal sulfides, 2) Sb-Ag minerals, and 3) the latest barren calcite, and also estimated temperatures (140–280°C) and pressures (f_{s_2} 10^{-13} – 10^{-20} bar) of Sb-Ag mineral by fluid inclusion microthermometry. Based on the decreasing trends of the hydrogen-oxygen isotope values observed, Choi (1998) suggested the involvements of meteoric fluids in the later hydrothermal stage in the Daejang deposit.

Whereas individual “deposit-scale” geological features in each of the deposits have been studied, no integrated “district-scale” magmatic-hydrothermal model has been established for the area. Based on systematic field observations and sample petrography studies, we confirmed the alteration patterns and ore mineralogies of the three deposits. After petrography, we performed a fluid inclusion study, which included systematic petrographic observations, microthermometry, laser Raman spectroscopy, and LA-ICP-MS microanalysis. By studying the fluid inclusions in mineralized quartz veins, we obtained information on pressure, temperature, and salinity and on trace element contents of the ore-bearing fluids in the three deposits. Based on the information obtained, we constructed a geologic-geochemical process for magmatic-hydrothermal fluids and ore mineralization in the deposits. Implications regarding mineralization potentials are discussed.

GEOLOGIC SETTINGS AND OVERVIEW OF THE DEPOSITS

Regional Geology

The Gyeongsang basin in the SE of the Korean Peninsula is a Cretaceous sedimentary basin formed in the Precambrian metamorphic basement (**Figure 1**). This basin is a tectonic pull-apart basin formed by northward oblique subduction of an ancient Izanagi oceanic plate into the Eurasian Plate during the Early Cretaceous. Subsequently, in the Late Cretaceous, the subduction angle became northwestward, and orthogonal subduction created an arc volcanism, called a Bulguksa orogeny (Chun and Chough, 1992; Chough et al., 2000; Lee et al., 2003; Ryu et al., 2006; Chough and Sohn, 2010). Bulguksa igneous rocks, generally granodioritic to granitic in composition, intrude into the Gyeongsang sedimentary basin. These are fine to coarse-grained porphyritic rocks mainly comprised of quartz, plagioclase, K-feldspar, biotite, and hornblende, and are classified as I-type magnetite series granitoid (Uchida et al., 2012).

Ryu et al. (2006) divided the Gyeongnam metallogenic belt into five stratigraphic units based on integrated stratigraphy, paleontology, paleomagnetism, geophysics, and age dating of igneous activities. They suggested a process for the formation of the Gyeongsang basin involving igneous activity caused by the direction and angle of subduction of the Izanagi plate. Koh et al. (2003) divided the Gyeongnam metallogenic belt into 3-period groups according to mineralization ages and directions of ore veins and suggested the direction of mineralization in the Gyeongsang basin proceeded from west to east connecting with the three groups with a belt of igneous activities in the SE part of China, the SE part of the Korean Peninsula, and the SW part of Japan.

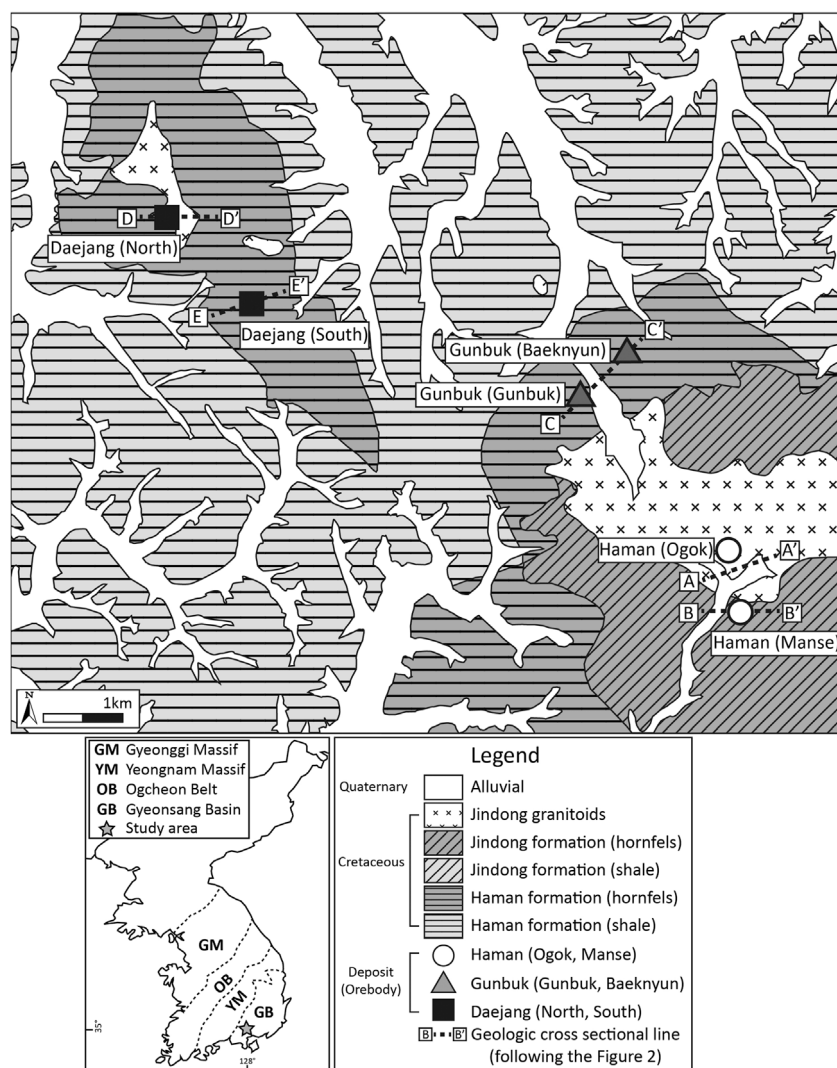


FIGURE 1 | Geological map of the Haman, Gunbuk, and Daejang deposits located in the Gyeongsang basin. The three deposits are hosted in the Cretaceous Haman-Jindong shale formation. The Haman-Jindong formation is widely metamorphosed into hornfels by an intrusion of Jindong granitoids. Geologic cross-sectional maps of the three deposits are shown in **Figure 2**.

The representative vein-type and breccia type deposits in the Gyeongnam metallogenic belt are as follows: vein-type deposits including the Haman-Gunbuk-Daejang deposits (Choi, 1985; Shin et al., 1987), Sambong-Samsan deposits (So et al., 1985), Kuryong-Cheongryong deposits (So et al., 1995), Donjeom deposit (Kim and Kim, 1974), and Keumryung-Gigu deposits (Park and Seol, 1992). The breccia-type deposits include the Ilgwang deposit (Yang and Jang, 2002; Seo, 2016) and Dalsung deposit (Won and Kim, 1966). The Sambong-Samsan, Kuryong-Cheongryong, and Donjeom deposits are hosted in shale-sandstones-conglomerates of the Cretaceous Hayang sedimentary group to an andesitic tuff-tuffaceous conglomerate-welded tuff of the Cretaceous Yuchon volcanoclastic group and show propylitic-potassic-argillic alterations (Kim and Kim, 1974; So et al., 1985; So et al.,

1995). The Keumryung-Gigu deposits are hosted in black shale of the Cretaceous Hayang sedimentary group to the rhyolite-andesitic tuff of the Tertiary volcanoclastic group and show propylitic-potassic-argillic alterations (Park and Seol, 1992). The Ilgwang and Dalsung deposits are hosted in andesitic tuff-tuffaceous conglomerate of the Cretaceous Yuchon volcanoclastic group and exhibit a propylitic-sericitic alteration (Won and Kim, 1966; Yang and Jang, 2002; Seo, 2016).

The Haman, Gunbuk, and Daejang deposits in the Gyeongnam metallogenic belt compose an Early to Late Cretaceous Sindong-Hayang sedimentary group, which is intruded by a series of Late Cretaceous Bulguksa magmas called Jindong granitoids (**Figure 1**). The Haman and Jindong shale formations belong to the Sindong-Hayang sedimentary group and are hosted in the Haman, Gunbuk, and Daejang

deposits. The Haman formation consists of conglomerate-sandstone, black sandstone, and reddish mudstone (Chang, 1977; Chang et al., 1998). The Jindong formation, which conformably overlays the Haman formation, consists of black shale, black mudstone, and siltstone (Kim, 1973). The Haman-Jindong shale formations are tilted at a strike of N45 ~ 70 E and a dip of 10 ~ 15 SE (Moon et al., 1970). The Jindong granitoids intrude into both Haman and Jindong formations and are composed of porphyritic-plutonic textured rocks such as granite, granodiorite, and quartz diorite. Granodiorite is the most widely observed igneous rock among the Jindong granitoids. The whole-rock K-Ar (Park et al., 1985; Shin et al., 1987) and zircon U-Pb (Kim et al., 2016a) ages of the Jindong granitoids (granodiorite) have been reported to be 88–97 and 90–91 Ma, respectively. The Jindong granitoid intrusion in the Gyeongsang basin is a magnetite-bearing I-type intrusion, which has been suggested to have caused copper mineralization in the Gyeongnam metallogenic belt, including the Haman, Gunbuk, and Daejang deposits (Park et al., 1983; Choi, 1985; Park et al., 1985; Shin et al., 1987; Lee, 1989; Lee et al., 1994; Koh et al., 2003). The Jindong granitoids have lower Rb and Ba contents and higher Sr contents than the neighboring Pb-Zn related granitoids (Lee and Moon, 1989), which suggests fertile granitoids with higher Cu-Pb-Zn and Cl contents of biotite than barren granitoids (Lee et al., 1994; Lee and Lee, 1994). The shale in the Haman and Jindong formations in studied areas is widely metamorphosed into hornfels by intrusions.

Deposit Overview and Sampling Strategy

The Haman and Gunbuk deposits are neighboring deposits spatially located in a small district (about 25 km²) in the SW part of the Gyeongnam metallogenic belt (35°13' 07.9309"N, 128°21' 41.7172"E ~ 35°11' 21.7"N, 128°23' 15.1"E) (**Figure 1**). They are hydrothermal vein-type Cu deposits with by-products of Au and Ag (Park et al., 1985; Heo et al., 2003). The estimated reserve of Cu ore in the Haman deposit is about 510 kt with an ore grade of 2–3 wt% of Cu (Kim, 1973). There are six orebodies in the Haman deposit, which are named Manse, Dundok, Namgok-Bukgok, Deokgok, Gilgok, and Ogok (**Figures 2A,B**). The strike/dip of ore veins in the Manse orebody are N15 ~ 70°W to N80 ~ 85°E and in the Ogok orebody are N20° ~ 30°E to 80° ~ 85°SE (Kim, 1973). The Gunbuk deposit is located 2 km to the NW of the Haman deposit. The estimated reserve of Cu ore in the Gunbuk deposit is about 960 kt (Kim, 1973). Joint and fault systems with a strike of N70°S to N15 ~ 30°W are related to ore distribution in the Gunbuk deposit (Kim, 1973). There are two major orebodies in this deposit, named the Gunbuk and Baeknyun orebodies (**Figure 2C**). The strike/slip of ore veins of the Gunbuk orebody is N5 ~ 20 to N80° ~ 90°W, and ore grades are 5–10 wt% for Cu, 15–20 g/t for Au, and 70–300 g/t for Ag (Kim, 1973). The strike/dip of the veins in the Baeknyun orebody are NS, N15° to S40° ~ 80°W, and the ore grades are 1–2 wt% for Cu, 7 g/t of Au, and 100–260 g/t for Ag (Kim, 1973). The Daejang deposit is a hydrothermal vein-type Cu deposit with minor Au and Ag components (Shin et al., 1987; Choi, 1998) (35°14' 05.9125"N, 128°18' 05.4025"E) located 5 km NW of the Gunbuk deposit. There is no record of ore reserves for the

Daejang deposit; joint and fault systems with a strike of NS to N20°W are related to ore distribution in this deposit (Kim et al., 2016b). The Daejang deposit has two orebodies, that is, North Cu-Pb-Zn-Au-Ag and South Cu-Au-Ag orebodies (**Figures 2D,E**). The strike/slip of ore veins of the North orebody is N15°W to 65° ~ 85°NE, with ore grades of ~0.11 wt% for Cu, 3–7 g/t for Pb, 2–5 g/t for Zn, ~0.4 g/t for Au, and 380–770 g/t for Ag (Kim et al., 2016b). The strike/slip of ore veins of the South orebody is N20°W to 80°SW, and ore grades are ~3.5 wt% for Cu, 1.4 g/t for Au, and 10–55 g/t for Ag (Kim et al., 2016b).

In the three deposits, we collected quartz vein samples showing a well-preserved texture of ore-alteration mineralogy and a crosscutting relationship. In the Haman deposit, we collected 31 quartz vein samples from the Manse and Ogok orebodies. In the Gunbuk deposit, we collected nine quartz vein samples from the Gunbuk and Baeknyun orebodies and some granodiorite outcrops. In the Daejang deposit, 10 quartz veins from the North and South orebodies, and some granodiorite outcrops were collected.

PETROGRAPHY

Ore and Alteration Minerals

Hornfels is widely formed (ca. 30 km²) in the Haman and Jindong formations around Jindong granitoid intrusions (**Figure 1**) and contain disseminated pyrite and magnetite. Magnetic susceptibilities ($\times 10^{-3}$ SI units) of the hornfels and granodiorite of Jindong granitoids in the region are about 50–60 and 17, respectively. The vein-bearing hornfels we studied commonly had pervasive chlorite and epidote alteration (CE alteration) before multiple veining events. In this section, we describe temporal relationships between hydrothermal alterations and paragenesis of ore-gangue mineral assemblages (**Figures 3–6**).

The major ore minerals of the Haman deposit include magnetite, pyrite, pyrrhotite, arsenopyrite, pyrite, and chalcopyrite, and minor ore minerals include scheelite, molybdenite, sphalerite, and galena. Quartz, tourmaline, actinolite, chlorite, and epidotes were observed as gangue minerals. We classified four veining stages in the Haman deposit: the first three quartz veining stages and the latest calcite veining stage. Hornfels in the Haman deposit has an early pervasive CE alteration. The hornfels with CE alteration was crosscut subsequently by a series of quartz veins hosting alterations of albite-actinolite (AA alteration) and tourmaline-biotite (TB alteration) (**Figure 3E**). Quartz veins accompanying an AA alteration are barren. Quartz veins are curvy and have thicknesses of 1–3 cm (**Figure 3E**). Quartz veins with TB alterations contain ore minerals and crosscut the earlier AA alteration (**Figures 3C,D**). These veins have thicknesses of 2–3 cm, but some veinlets are less than 1 cm. We classified two separate stages among the quartz veins with TB alterations. Earlier ones have massive oxide and sulfide ore minerals of magnetite-tourmaline-chalcopyrite-pyrite with disseminated scheelite-molybdenite in the vein. Later ones accompany minor K-feldspar with TB alteration, which has similar mineralogy but is richer in sulfide minerals. The veins show tourmaline-pyrrhotite-chalcopyrite-pyrite-arsenopyrite with

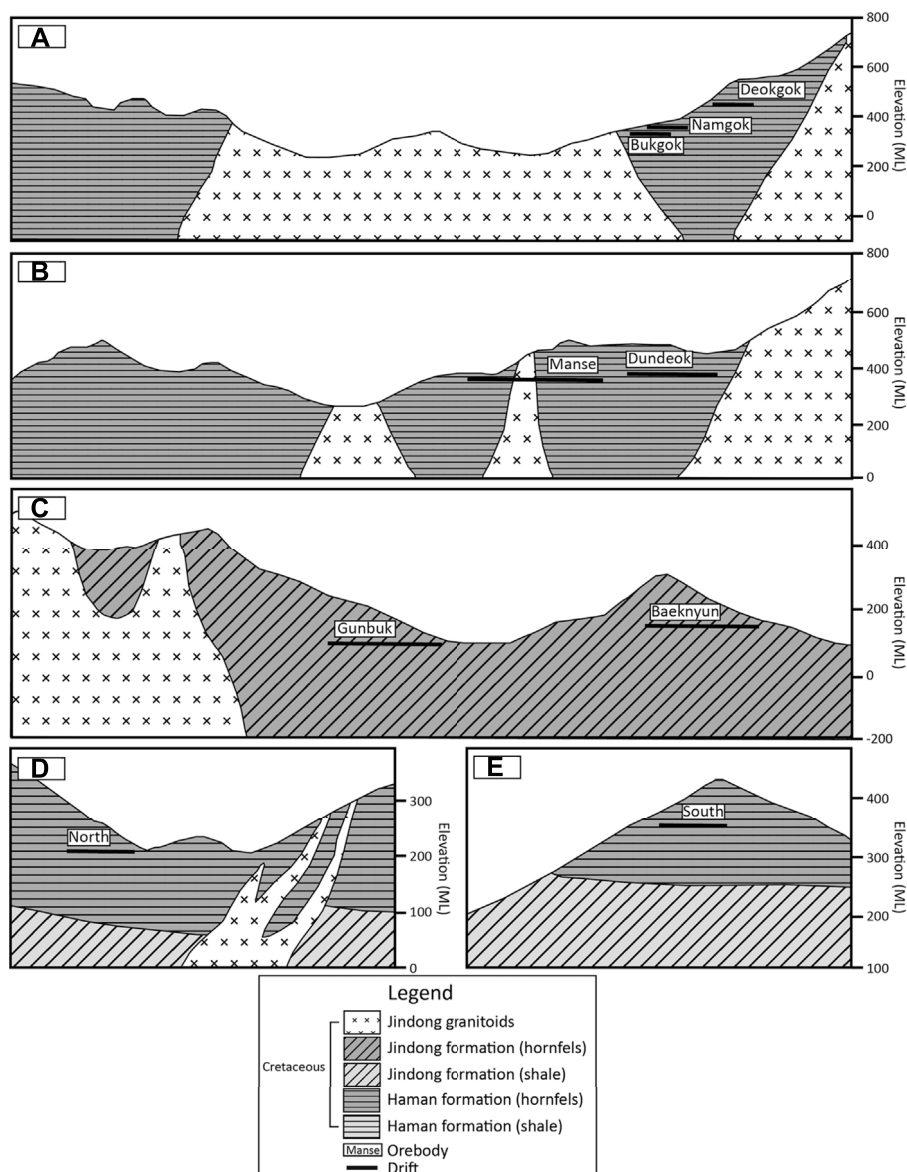


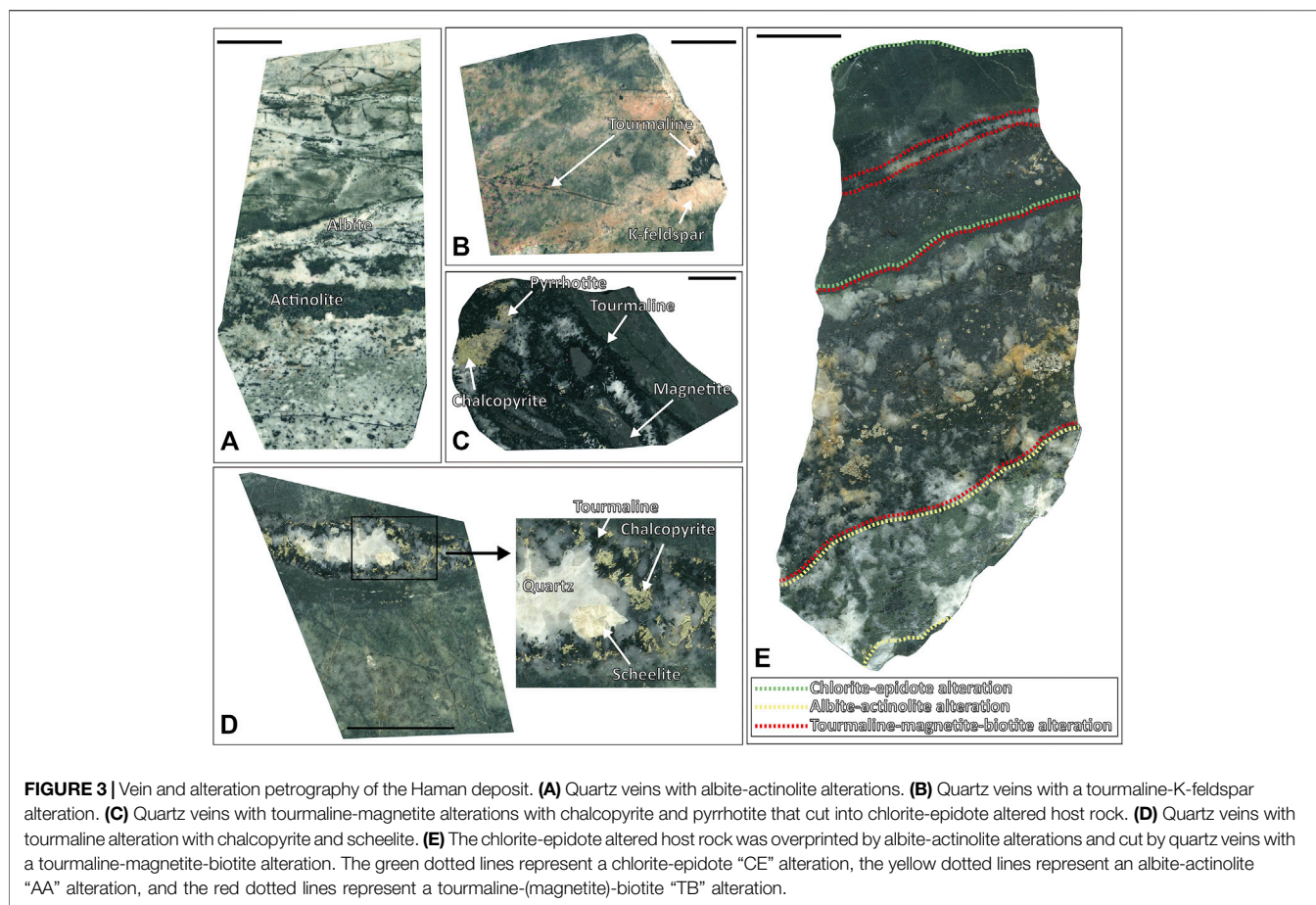
FIGURE 2 | Geologic cross-sections of the Haman, Gunbuk, and Daejang deposits. **(A)** Namgok-Bukgok orebody of the Haman deposit. The Ogok orebody is located near the Namgok-Bukgok orebody surrounded by Jindong granitoids. **(B)** Manse and Dundeok orebody of the Haman deposit. **(C)** Gunbuk-Baeknyun orebody of the Gunbuk deposit. **(D)** North orebody of the Daejang deposit. **(E)** South orebody of the Daejang deposit. The maps are modified versions of those produced by Moon et al. (1986), Kim et al. (2016b).

minors of magnetite-galena-sphalerite (Figures 3E, 6A). No scheelite-molybdenite was observed in the later quartz vein with TB alteration. The latest stage is a calcite vein with disseminated chalcopyrite, and it crosscuts previous quartz veins (Supplementary Table S1, Figures 3, 6A).

In the Gunbuk deposit, we observed magnetite, arsenopyrite, pyrrhotite, pyrite, and chalcopyrite as major ore minerals with sphalerite and galena as minor minerals. Quartz, tourmaline, and calcite were observed as gangue minerals. There are two veining stages in the Gunbuk deposit; a mineralized quartz vein and a postdating barren calcite vein. A pervasive CE alteration also appeared in hornfels before the quartz vein with TB alteration

(Figure 4B). Unlike the Haman deposit, AA alteration was absent in Gunbuk veins. The quartz veins are 1–2 cm thick and have ore minerals including massive magnetite, pyrrhotite, chalcopyrite, pyrite, arsenopyrite, sphalerite, and galena. Unlike the Haman deposit, the oxide-sulfide ores in the quartz veins occur together in the Gunbuk deposit. Sphalerite and galena were more commonly observed in the Gunbuk veins than in the Haman veins. Second stage calcite veins were barren and crosscut previous quartz veins (Supplementary Table S1 and Figures 4, 6B).

The Daejang deposit, which is geographically removed from the Haman and Gunbuk deposits, contains a distinct ore mineral assemblage. They are Pb-Zn rich and contain no magnetite.



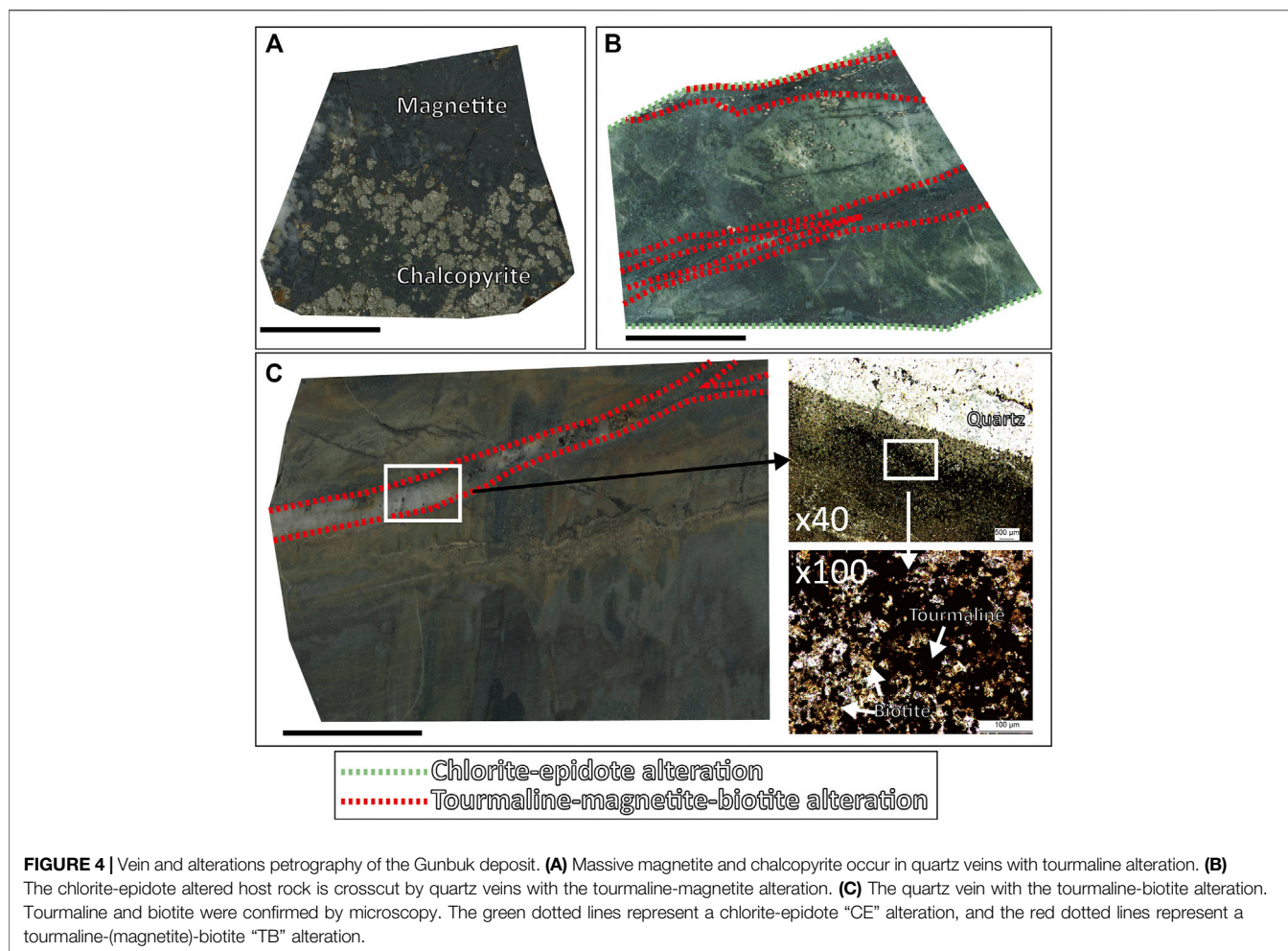
Pyrrhotite, arsenopyrite, pyrite, chalcopyrite, sphalerite, and galena were observed as ore minerals, and quartz, and calcite as gangue minerals. Two stages of veins were identified in the Daejang deposit: earlier quartz veins with TB alterations and a later calcite vein stage. A pervasive CE alteration was also observed in hornfels, crosscut by a series of mineralized quartz veins with TB alteration. The quartz veins were 1–3 cm thick and hosted ore mineralization. In the Daejang deposits, TB alterations that developed along quartz veins were generally thinner (<1 cm) than in the Haman and Gunbuk deposits (Figure 5B). The quartz veins have massive chalcopyrite-pyrite-sphalerite-galena with minor pyrrhotite-arsenopyrite (Figure 5C). Unlike the Haman and Gunbuk deposits, the Daejang deposit hosts massive sphalerite and galena in quartz veins. It has been reported that some Sb-bearing minerals such as gudmundite and boulangerite are also present in the Daejan deposit (Shin et al., 1987; Park and Kim, 1988; Choi, 1998). The latest thin (<1 cm) and barren calcite veins crosscut former quartz veins (Supplementary Table S1 and Figure 6C).

A summary of the mineral and alteration paragenesis in the three deposits is provided in Figure 6D. The three deposits show common veining and alteration features: earlier CE alterations in hornfels, crosscutting quartz veins with TB alteration associated with oxide-sulfide mineralization, and the latest calcite veins.

Fluid Inclusion Assemblages

Ore-mineralized main-stage quartz veins were selected to study fluid inclusion. The sizes of the inclusions vary from ~5 to 30 μm in diameter. We petrographically described the pseudosecondary fluid inclusion assemblage (FIA) (Figure 7) textural co-genetic group of fluid inclusions (Goldstein and Reynolds, 1994; Bodnar, 2003a), for subsequent microthermometry and microanalysis. We classify three types of fluid inclusions: 1) aqueous liquid-rich "liquid" inclusions (Figure 7A, 7D, 7G), 2) aqueous vapor-rich "vapor" inclusions (Figure 7C, 7F, 7I) aqueous halite-bearing "brine" inclusions (Figure 7B, 7E, 7H). Liquid inclusions had a bubble size of 10–50 vol% (commonly about 20%) and homogenized into a liquid phase. Vapor inclusions had a bubble size of 70–80 vol% and homogenized into a vapor phase. Brine inclusions contained daughter crystals of salts (possibly NaCl and KCl). Some brine inclusions were associated and co-trapped with vapor inclusions in a single assemblage (a boiling assemblage) (Figure 7J).

We observed varying distributions and proportions of fluid inclusion types in each deposit and orebody (Supplementary Table S2) Brine inclusions predominated in the Haman deposit (ca. > 50%), whereas liquid and vapor inclusions accounted for less than about 20 and 30%, respectively. In the Gunbuk deposit, brine inclusions accounted for ~30%, liquid inclusions ~40% and for ~30% of vapor inclusions. In



the Daejang deposit corresponding values were 40, 30, and 30%, respectively.

METHODS

Fluid Inclusion Microthermometry

Fluid inclusion microthermometry was performed on doubly polished quartz chips from the 13 quartz vein samples obtained from each of the three deposits. A total of 133 FIAs (about 300 single fluid inclusions) were studied, that is, 50 from the Haman deposit, 41 from the Gunbuk deposit, and 42 from the Daejang deposit. Fluid inclusion microthermometry was carried out using a Linkam FTIR 600 heating-freezing stage at Inha University, which was calibrated using synthetic fluid inclusions of H₂O and CO₂-H₂O. The freezing and heating procedures were conducted at accuracies of ± 0.1 and $\pm 1^\circ\text{C}$, respectively. Final ice melting and final halite melting temperatures were measured to calculate apparent salinities (NaCl equivalent wt%) (Bodnar and Vityk, 1994). Calculated salinities and homogenization temperatures (T_h) were combined to calculate a minimum trapping pressure and an isochore using a model NaCl-H₂O system (Driesner and Heinrich, 2007). An average ± 1 sigma was calculated for single fluid inclusions in the FIA (Supplementary Table S3).

Raman Spectroscopy

Laser Raman spectroscopy was performed on the bubble parts in vapor inclusions to identify gases in the fluids. A LabRam HR Evolution confocal Raman spectrometer (HORIBA) in Inha University was used, which was equipped with an 1800 g mm⁻¹ grating, a 100x confocal lens, and an edge filter. Raman spectra were obtained at a laser excitation wavelength of 532 nm (green laser), a laser power of 2 mW, filtering between 25 and 50%, a beam diameter of 100 μm , an acquisition time of 5 s, accumulation of 3–20 times, and a spectral range of 600–4,200 cm⁻¹. Twelve vapor inclusions from the Haman deposit, 21 from the Gunbuk deposit, and 13 from the Daejang deposit were analyzed.

Laser Ablation-ICP-MS Microanalysis of Fluid Inclusions

LA-ICP-MS microanalysis of brine inclusions in quartz veins was conducted after microthermometry using an LA-ICP-MS system at the Korea Polar Research Institute (KOPRI). The system had a 193 nm ArF Excimer laser (ESI NWR 193 model) connected to a quadrupole ICP-MS (iCAP-Q model). 116 single fluid inclusions from 70 FIAs were analyzed. Laser beam sizes were adjusted to the diameters of inclusions to fully evacuate all components in the

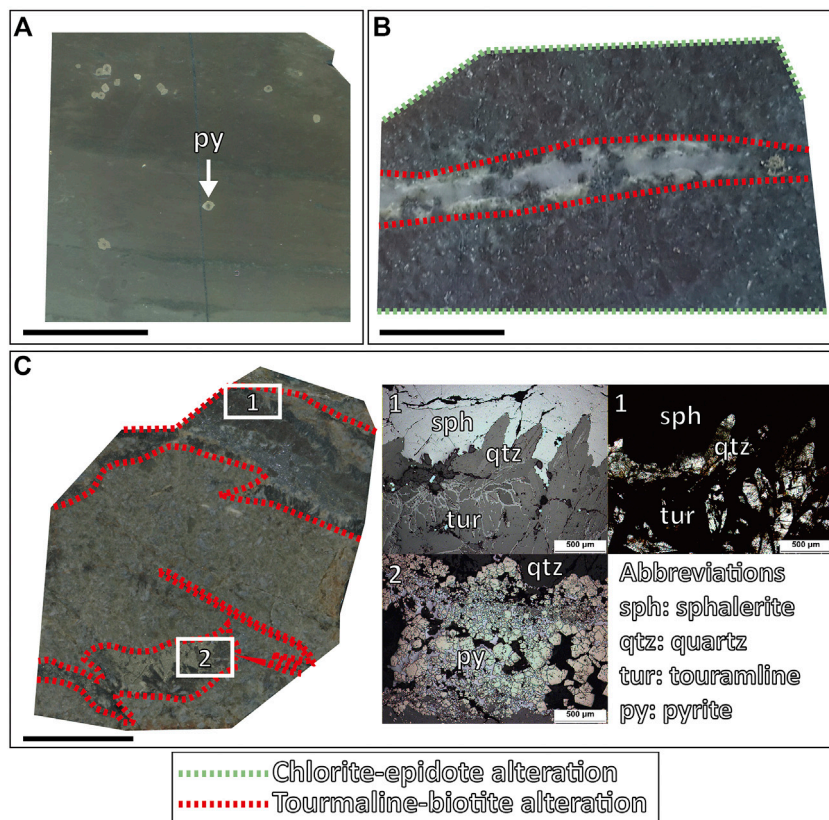


FIGURE 5 | Vein and alterations petrography of the Daejang deposit. **(A)** Pyrite grains are present in hornfels. **(B)** Tourmaline-(K-feldspar)-biotite alterations are shown along the quartz veins cutting the chlorite-epidote altered host rock. **(C)** Tourmaline-biotite alterations formed along the quartz veins. (C-1) Tourmaline, sphalerite, quartz, and (C-2) pyrite images obtained by reflected (**left**) and transmitted light (**right**) microscopy. The green dotted lines represent a chlorite-epidote “CE” alteration, and the red dotted lines represent a tourmaline-(magnetite)-biotite “TB” alteration.

brine inclusions. The laser energy density used was 7–8 J/cm² and 3–10 Hz repetition rates were applied. To analyze inclusions and hosting quartz, we used 10 ms dwell times for the following isotopes; ¹¹B, ²³Na, ²⁷Al, ²⁹Si, ³⁹K, ⁴⁰Ca, ⁴⁹Ti, ⁵⁵Mn, ⁵⁷Fe, ⁶⁵Cu, ⁶⁶Zn, ⁷⁵As, ⁸⁵Rb, ⁸⁸Sr, ¹³³Cs, and ²⁰⁸Pb. A standard reference material (SRM) of NIST 610 glass was used as an external standard to calculate element ratios. Empirical estimation of Na concentrations from fluid inclusion salinities (Heinrich et al., 2003) was applied as an internal standard. Data reductions and quantifications from convoluted transient signals of fluid inclusions (**Figure 8**) were carried out using SILLS software (Guillong et al., 2008). During the ablations of hosting quartz, trace elements, including Ti and Al, in the quartz were simultaneously analyzed.

RESULTS

Microthermometry and Calculation of Pressure

Ranges of salinities and T_h values obtained from liquid inclusion assemblages were found to be highly overlapping (**Figures 9A, 10**). T_h values from liquid inclusion assemblages were 96–360°C in the Haman deposit, 200–310°C in the Gunbuk deposit, and

150–290°C in the Daejang deposit. Salinities in liquid inclusion assemblages were 2–19 wt% in the Haman deposit, 3–18 wt% in the Gunbuk deposit, and 6–17 wt% in the Daejang deposit (**Supplementary Table S3**).

T_h values of brine inclusion assemblages were 340–600°C in the Haman deposit, 250–470°C in the Gunbuk deposit, and 320–460°C in the Daejang deposit. Salinities in the brine inclusion assemblages are 33–62 wt% in the Haman deposit, 34–59 wt% in the Gunbuk deposit, and 39–55 wt% in the Daejang deposit. Fluid pressures of each deposit were calculated from salinities and T_h values obtained from brine inclusions. Maximum pressures of the Haman, Gunbuk, and Daejang deposits were 500, 330, and 270 bar, respectively. T_h values and calculated pressures were highest for the Haman deposit and similar for the Gunbuk and Daejang deposits (**Figure 9B**).

Raman Spectroscopy

Gas species were detected in the bubbles of vapor inclusions (**Figure 11**). CO₂ peaks were identified in the Ogok (Haman), Baeknyun (Gunbuk), Gunbuk (Gunbuk), North (Daejang), and outcrop (Daejang) orebodies, and CH₄ peaks were detected in the Gunbuk (Gunbuk) orebody and outcrop (Daejang).

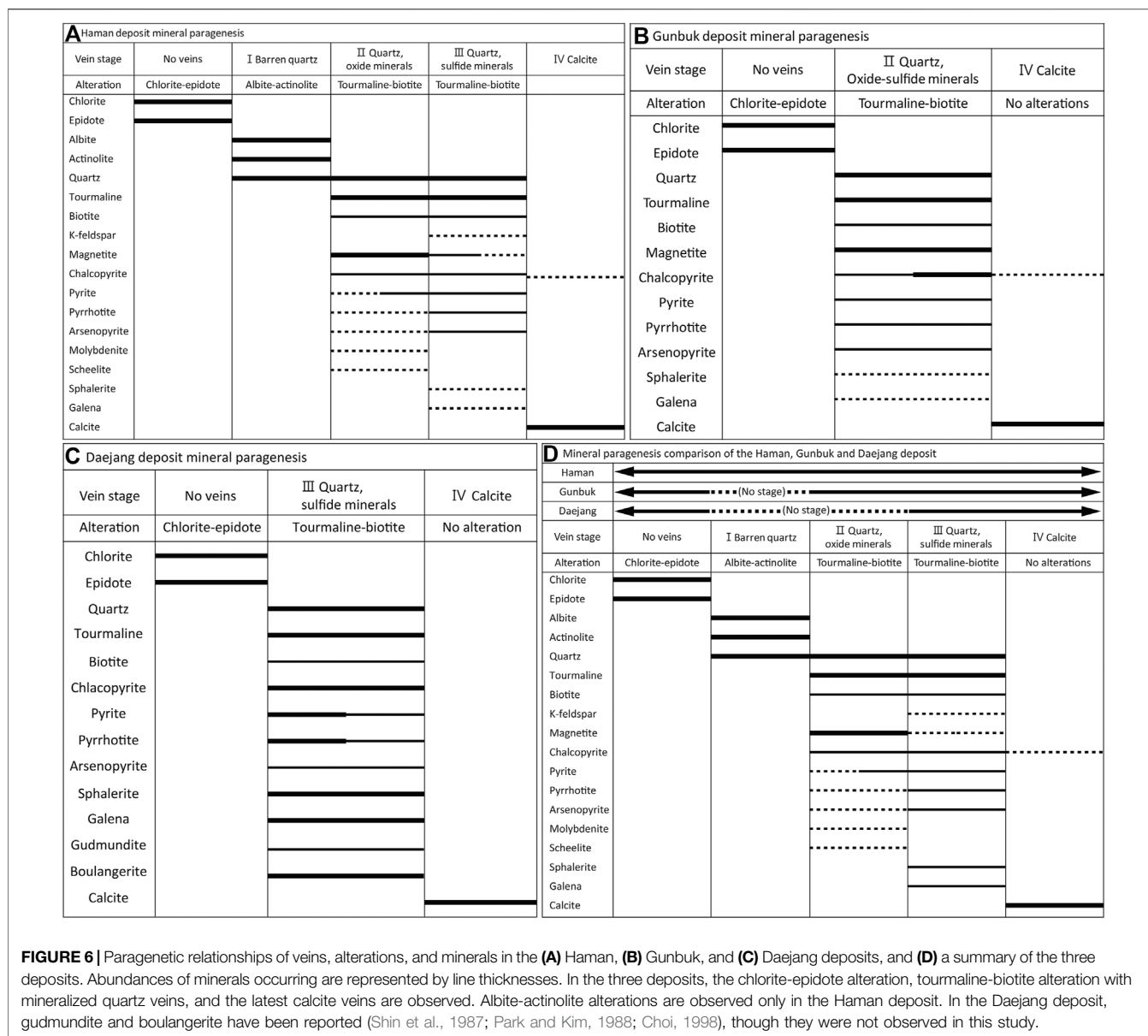


FIGURE 6 | Paragenetic relationships of veins, alterations, and minerals in the (A) Haman, (B) Gunbuk, and (C) Daejang deposits, and (D) a summary of the three deposits. Abundances of minerals occurring are represented by line thicknesses. In the three deposits, the chlorite-epidote alteration, tourmaline-biotite alteration with mineralized quartz veins, and the latest calcite veins are observed. Albite-actinolite alterations are observed only in the Haman deposit. In the Daejang deposit, gudmundite and boulangerite have been reported (Shin et al., 1987; Park and Kim, 1988; Choi, 1998), though they were not observed in this study.

Trace Elements in Quartz

All levels in quartz at the Haman, Gunbuk, and Daejang deposits were 70–510, 40–600, and 30–230 ppm, respectively (Supplementary Table S4 and Figure 12A), and corresponding values for Ti were 12–140, 4–55, and 5–56 ppm (Supplementary Table S4 and Figure 12B).

Trace Elements in Brine Inclusion Assemblages

Rb, Sr, Cs, Mn, Fe, Zn, and Pb signals in brine inclusions were obvious (Figure 8), whereas signals of other elements were not clear because of high background levels in gas blanks and quartz matrices. Concentrations of Cs, Mn, Pb, Fe, and Zn, and Rb/Sr and Fe/Mn ratios in brine inclusion assemblages are provided in Figure 13 and

Supplementary Table S5. The range of Rb/Sr ratios and Cs concentrations in brine inclusion assemblages of the Haman, Gunbuk, and Daejang deposits were 0.1–1.0 and 10–240 ppm, 0.1–0.8 and 20–340 ppm, and 0.2–16 and 50–1,250 ppm, respectively. The Haman and Gunbuk deposits had similar Cs concentrations and Rb/Sr ratios, whereas the Daejang deposit had higher values. The metal concentrations (ppm) in the brine assemblages of the Haman deposit were 3 ~ 20 k for Mn, 20 ~ 100 k for Fe, 100 ~ 5 k for Zn, and 200 ~ 2 k for Pb, in the Gunbuk deposit were 2 ~ 20 k for Mn, 10 ~ 100 k for Fe, 300 ~ 5 k for Zn, and 100 ~ 2 k for Pb are in the brine assemblages, and in the Daejang deposit were 7 ~ 50 k for Mn, 10 ~ 100 k for Fe, 3 ~ 15 k for Zn, and 2 ~ 10 k for Pb are in the brine assemblages. Mn concentrations and ranges were comparable in all deposits, whereas concentrations of Fe, Zn, and Pb were much higher in the Daejang deposit.

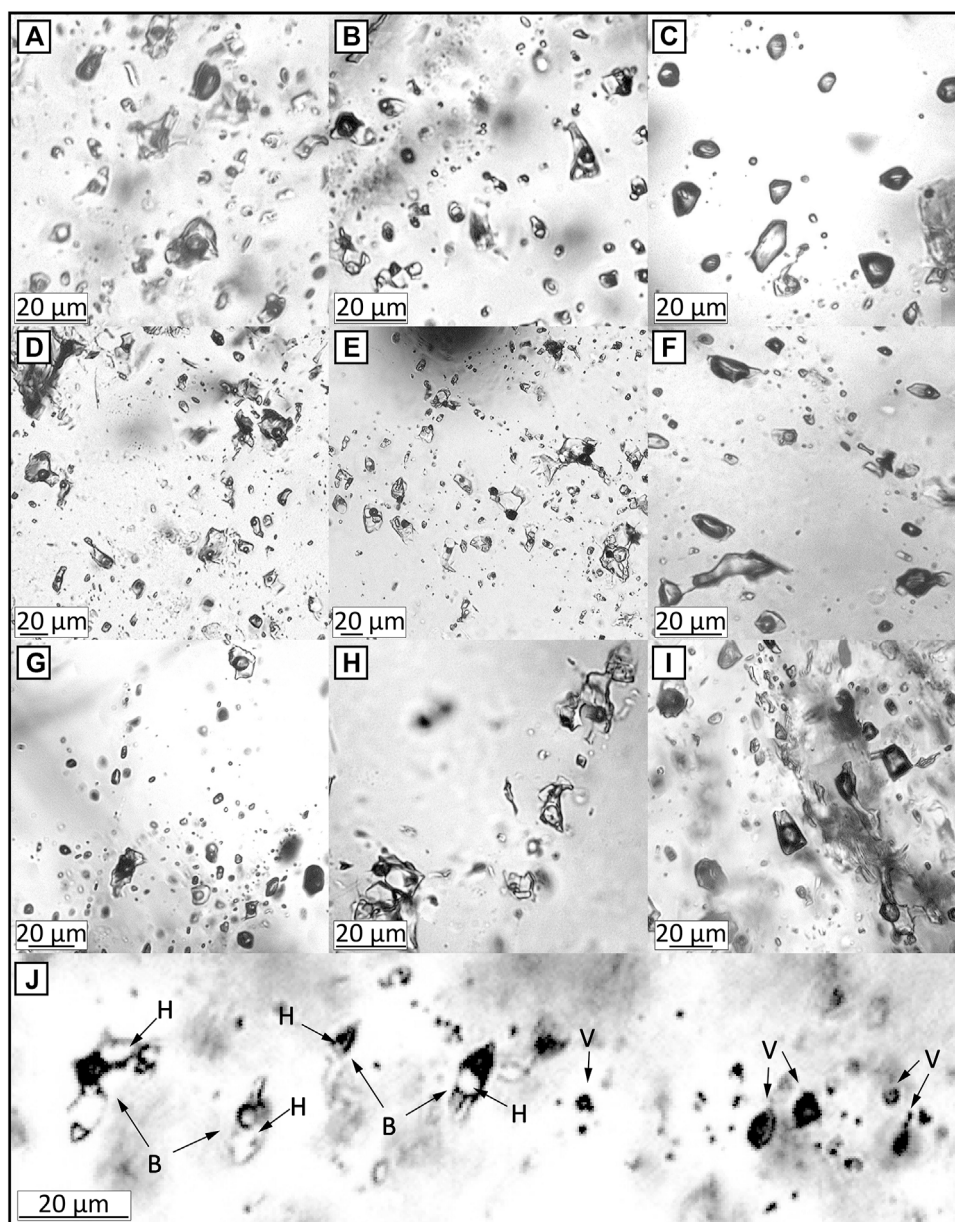


FIGURE 7 | Types of fluid inclusion assemblages in mineralized quartz veins. (A) liquid inclusions, (B) brine inclusions, and (C) vapor inclusions in the Haman deposit. (D) liquid inclusions, (E) brine inclusions, and (F) vapor inclusions in the Gunbuk deposit. (G) liquid inclusions, (H) brine inclusions, and (I) vapor inclusions in the Daejang deposit. (J) The brine and vapor inclusions in the boiling assemblage in the Daejang deposit. B, V, and H represent brine inclusion, vapor inclusion, and halite, respectively. Most of the fluid inclusions observed in the studied deposits were either liquid inclusions with a bubble size of around 20 vol% or brine inclusions with a bubble size of 10–30 vol%. Minor vapor inclusions with bubble sizes of 70–80 vol% were also observed.

DISCUSSION

Origin of Alterations and Ore Mineral Assemblages

Based on petrographic features such as vein-cross cutting, alteration, and ore mineral assemblages in the Haman, Gunbuk, and Daejang deposits, we classify their common paragenetic sequences as follows: 1) an early barren pervasive CE alteration overprinting hornfels, 2)

main-stage quartz veins of the TB alteration mineralized with chalcopyrite-pyrite-arsenopyrite (\pm magnetite-pyrrhotite-sphalerite-galena), and 3) the latest barren calcite vein. The main-stage TB alteration was often associated with the AA alteration in the Haman deposit and with K-feldspar in the Haman, Gunbuk, and Daejang deposits.

The Haman-Jindong hornfels was formed by magmatism of the Jindong granitoids (Park et al., 1985; Shin et al., 1987).

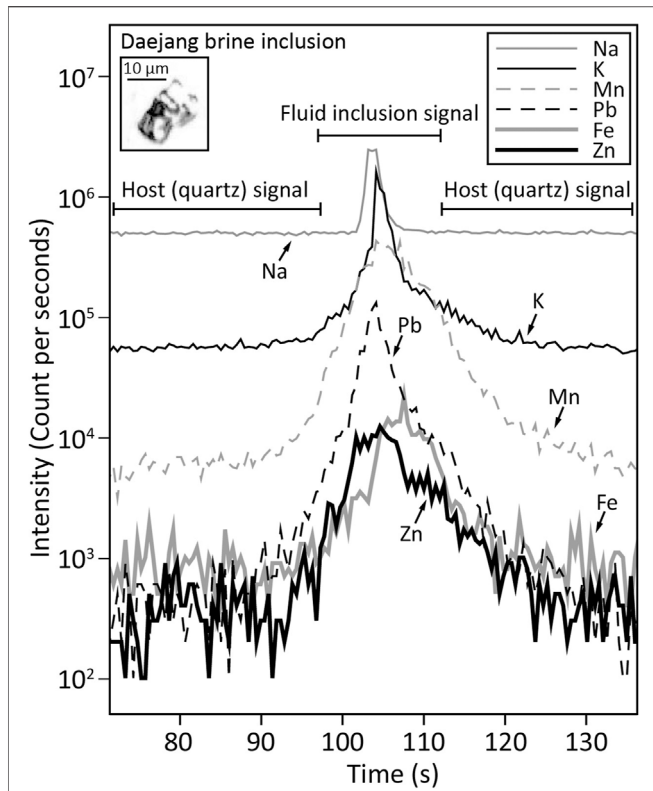


FIGURE 8 | Transient signals of LA-ICP-MS of brine inclusions analysis (Daejang quartz veins) showing signals for Si, Na, Mn, Pb, Fe, and Zn.

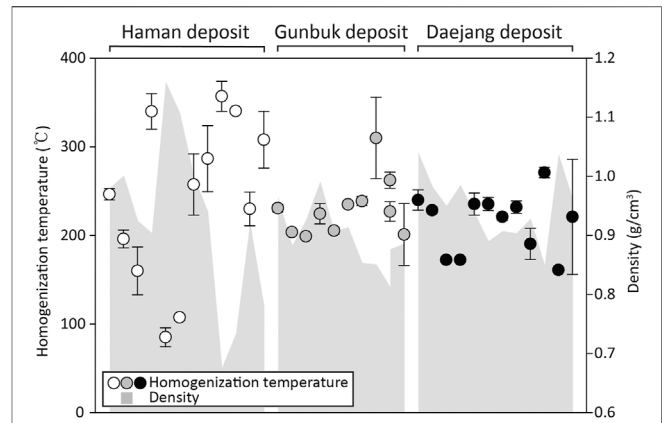


FIGURE 10 | Homogenization temperature and density plots of liquid inclusion assemblages. The Gunbuk and Daejang deposits have similar densities and temperature ranges, whereas the Haman deposit has broader and higher average ranges.

Magnetic susceptibilities (SI unit) in the hornfels were significantly higher ($50\text{--}60 \times 10^{-3}$) than in granitoids (granodiorite; $15\text{--}17 \times 10^{-3}$ and pegmatite; $2\text{--}4 \times 10^{-3}$). Although we cannot observe under a microscope, we estimated that the hornfels contained disseminated micro-particles of magnetite. Observations of disseminated pyrite in Haman-Jindong hornfels (**Figure 5A**) and unmetamorphosed Haman-Jindong shale (Kim and Paik, 2001; Kim et al., 2018) indicated that the Fe from the Haman-Jindong parent shale was

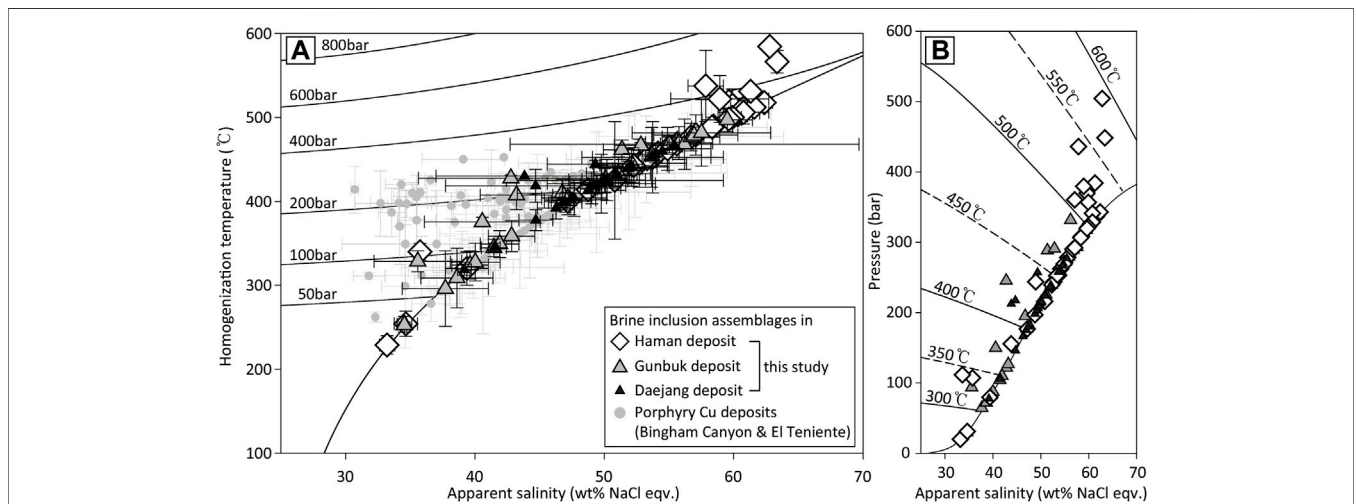
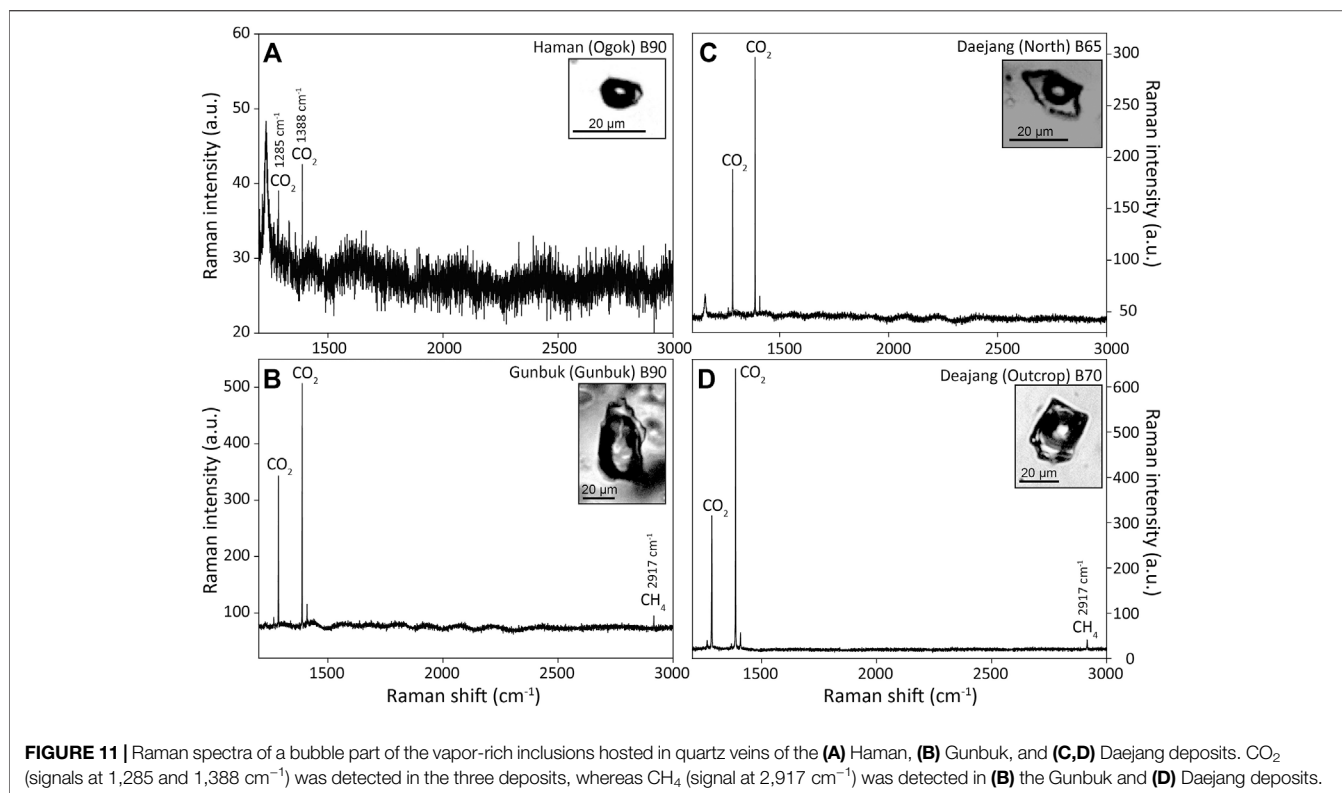


FIGURE 9 | **(A)** Plots of homogenization temperatures versus apparent salinities (NaCl wt.% equivalents) obtained from brine assemblages of the Haman, Gunbuk, Daejang deposit and porphyry-style deposits (Bingham Canyon & El Teniente deposit) (Klemm et al., 2007; Landtwing et al., 2010). The gray circles represent the porphyry deposits, the white diamonds represent the Haman deposit, the gray triangles represent the Gunbuk deposit, and the black triangles represent the Daejang deposit. Ranges of the Gunbuk and Daejang deposits partially overlap with porphyry deposits, maximum temperatures were exceptionally higher in the Haman deposit than in porphyry deposits. **(B)** Plots of salinity versus calculated pressure for brine inclusion assemblages in the three deposits. The circles represent liquid inclusion assemblages, and the rhombus and triangle symbols represent brine inclusion assemblages. White circles and rhombus symbols represent T_h and salinity of the Haman deposit, gray circles and triangles represent T_h and salinity of the Gunbuk deposit, and black circles and triangles represent T_h and salinity of the Daejang deposit.



probably the source of the formation of disseminated magnetite in hornfels. Whereas massive precipitation of magnetite was present in the quartz veins of the Haman and Gunbuk deposits (Figure 3C and Figure 4A), and magnetite did not precipitate in the Daejang deposit, which may have been due to different temperature and sulfidation conditions of the magmatic-hydrothermal fluids (Einaudi et al., 2003) in the Haman, Gunbuk, and Daejang deposits. The quartz veins with the TB alteration in the Daejang deposit contained massive sulfide minerals such as pyrrhotite, pyrite, galena, and sphalerite, instead of magnetite (Figure 5C), whereas Fe concentrations in the brines of all three deposits were comparable (Supplementary Table S5). These contrasting Fe mineral precipitations might be due to relatively lower hydrothermal temperatures, which agrees with our fluid inclusion results (Figures 9, 10), and suggests the possibility of higher sulfidation states of magmatic-hydrothermal fluids in the Daejang deposit as compared with the Haman and Gunduk deposits (Figure 14) (Einaudi et al., 2003; Reed and Palandri, 2006).

The CE alteration which occurs exclusively along the margin of the Jindong granitoids (Choi, 1998; Heo et al., 2003) indicates that the alteration is strongly associated with the intrusions. A CE alteration can be formed either by a convection of external fluids driven by magmatism (Seedorff et al., 2005; Ayuso et al., 2010; Sillitoe, 2010), or by a cooled magmatic fluids (Orovan et al., 2018; Pacey et al., 2020). The geochemical studies on the alteration minerals (e.g. chlorite, epidote) are required to trace

the origin of the alteration and use it as an exploration target in the area (Wilkinson et al., 2020).

An AA alteration (Figure 3A) occurs exclusively in the Haman deposit. The AA alteration, which is associated with Na-Ca rich alteration minerals, is often observed in the barren and lower part of Cu ore bodies of porphyry deposits (Carten, 1986; Dilles and Einaudi, 1992; Dilles et al., 2000; Sillitoe, 2010) or in some Iron-Oxide-Copper-Gold (IOCG) deposits (Barton and Johnson, 2004; Williams et al., 2005), in which replacing K-feldspar into Na plagioclase or epidote, and biotite or hornblende into Ca amphibole (actinolite) (Dilles and Einaudi, 1992). The existence of the AA alteration suggests that the Haman deposit may have been formed deeper than the Gunbuk and Daejang deposits, which is in line with our fluid inclusion results. The origins of AA alteration, which can be referred to as a Na-Ca alteration, occurring in some of the magmatic-hydrothermal ore deposits have been suggested to be either externally-derived salty fluids (Dilles and Einaudi, 1992; Barton and Johnson, 1996; Xavier et al., 2008) or magmatically-derived fluids (Oliver, 1996; Pollard et al., 1997a; Mark and Foster, 2000; Perring et al., 2000). In the Haman deposit, pervasive CE alterations occurred after the metamorphism of hornfels due to granitoid intrusions, and quartz veins with AA alterations cut through the CE alternations (Figure 3A). The alteration and crosscutting relationship feature in the Haman deposit suggests that the AA alteration might have formed due to a magma-derived fluid from Jindong granitoids, but we cannot rule out the

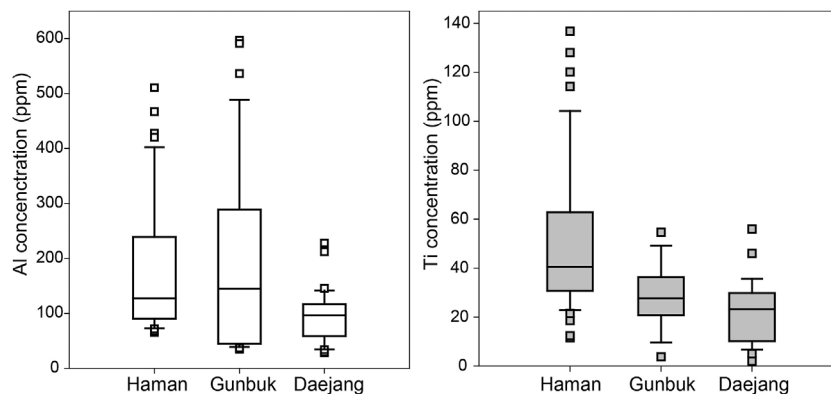


FIGURE 12 | Concentrations and ranges for **(A)** Al and **(B)** Ti concentrations in the quartz veins of the Haman, Gunbuk, and Daejang deposits. Ranges of Al concentrations in the Haman and Gunbuk deposits overlapped, and ranges of Ti concentrations in the Gunbuk and Daejang deposits also overlapped.

possibility of heated externally derived water from pores of the surrounding Haman-Jindong shale formations.

Occurrence of scheelite-molybdenite (**Figure 3D**) in the Ogok orebody of the Haman deposit indicates an elevated W-Mo concentration in magmatic-hydrothermal fluids, which can be related to a significantly fractionated magma (Kooiman et al., 1986; Seedorff et al., 2005; Sinclair, 2007). This differentiated, possibly granitic, magma might be occur at depth, while outcrops of the Jindong granitoids show a rather intermediate magmatic composition ranging from gabbro to granodiorite (Wee et al., 2007).

Like biotite, tourmaline was a commonly observed alteration mineral in the mineralized veins of all deposits (TB alteration: **Figures 3C, 4C, 5C**), and the quartz veins associated with tourmaline contained boiling assemblages indicating fluid phase separation (**Supplementary Table S3**). Tourmaline is commonly associated with many alteration types such as Na-Ca, K, and phyllic alterations in porphyry deposits (Sillitoe and Sawkins, 1971; Gustafson and Hunt, 1975; Dilles and Einaudi, 1992). Lynch and Ortega (1997) suggested that the precipitation of tourmaline can be promoted by phase separation of magmatic-hydrothermal fluids rich in boric acid derived from a fractionated B-rich granite. B is abundant in oceanic sediments and in altered oceanic crust and has a relatively high solubility in fluids, which results in B-rich arc magma (Moran et al., 1992; Leeman et al., 1994; Dreyer et al., 2010). Abundant tourmaline in the deposits studied suggests a B-rich causative magma and B-rich magmatic fluids in the area. The Gukjeon Pb-Zn deposit, which is located 55 km NE from the Haman, Gunbuk, and Daejang deposits, contains abundant axinite [(Ca, Fe, Mn)₃Al₂BO₃Si₄O₁₂(OH)] as a major skarn mineral, and its B has been suggested to originate from Late Cretaceous arc magma (Kim et al., 2021).

P-T Conditions and the Geochemistry of Hydrothermal Fluids

The presence of boiling assemblages suggests fluid phase separation due to a rapid depressurization, which commonly occurs in magmatic-hydrothermal deposits (Audétat et al., 1998;

Heinrich et al., 1999). Many boiling assemblages have been reported in quartz veins in the three deposits, and these could provide the actual P-T conditions of hydrothermal fluids (Roedder and Bodnar, 1980). A density contrast between brine and vapor in boiling assemblages indicates degrees of depressurization during phase separation. Pressures calculated from brine analysis results of boiling assemblages can be converted into paleodepths based on lithostatic (density of 2.7 g/cm³) or hydrostatic (density of 1.0 g/cm³) pressure regimes. In the Haman deposit, the apparent paleodepths calculated from lithostatic and hydrostatic pressure regimes were 0.5–2.0 and 1.3–5.4 km, in the Gunbuk deposit were 0.1–1.2 and 0.2–3.2 km, and in the Daejang deposit were 0.3–1.0 and 0.8–2.7 km, respectively (**Supplementary Table S3**).

Since the Fe (Fe²⁺ → Fe³⁺) oxidation has a faster reaction rate than Mn (Mn²⁺ → Mn⁴⁺), Fe/Mn ratio can be used as a redox indicator of fluid passing through a fluid-rock buffered system (i.e. the Fe/Mn ratio is lower for an oxidizing fluid) (Boctor, 1985; Naehrer et al., 2013). Bottrell and Yardley (1991) reported an increasing trend for Fe/Mn ratio when fluids at equilibrium with chlorite react with the reduced host rock, and Seo et al. (2012) showed a reducing fluid evolution from Cu-stage to Mo-stage in a porphyry deposit when Fe/Mn ratios in brines were increased. Fe/Mn ratios in brine inclusions were found to be lower in the Daejang deposit than in the Haman and Gunbuk deposits (**Figure 13C**), which suggests a relatively oxidizing fluid in the Daejang deposit. CO₂ was detected by Raman spectroscopy in some vapor inclusions (**Figure 11**), whereas clathrate was not observed by fluid inclusion microthermometry. Choi (1985) and Heo et al. (2003) reported that CO₂ was not detected in fluid inclusions of the Haman and Gunbuk deposits, whereas Choi (1998) reported a carbonic liquid phase in fluid inclusions of the Daejang deposit. CO₂ contents in fluids might have increased fluid carbonate activity in the fluids and formed the latest calcite vein (Choi, 1998). CH₄ was detected in fluid inclusions in the Gunbuk and the Daejang deposits by Raman spectroscopy (**Figure 11**). The ratios of mole fractions of CO₂ and CH₄ in fluid inclusions have been used to reconstruct fluid redox conditions (Giggenbach, 1987; Dubessy et al., 1989;

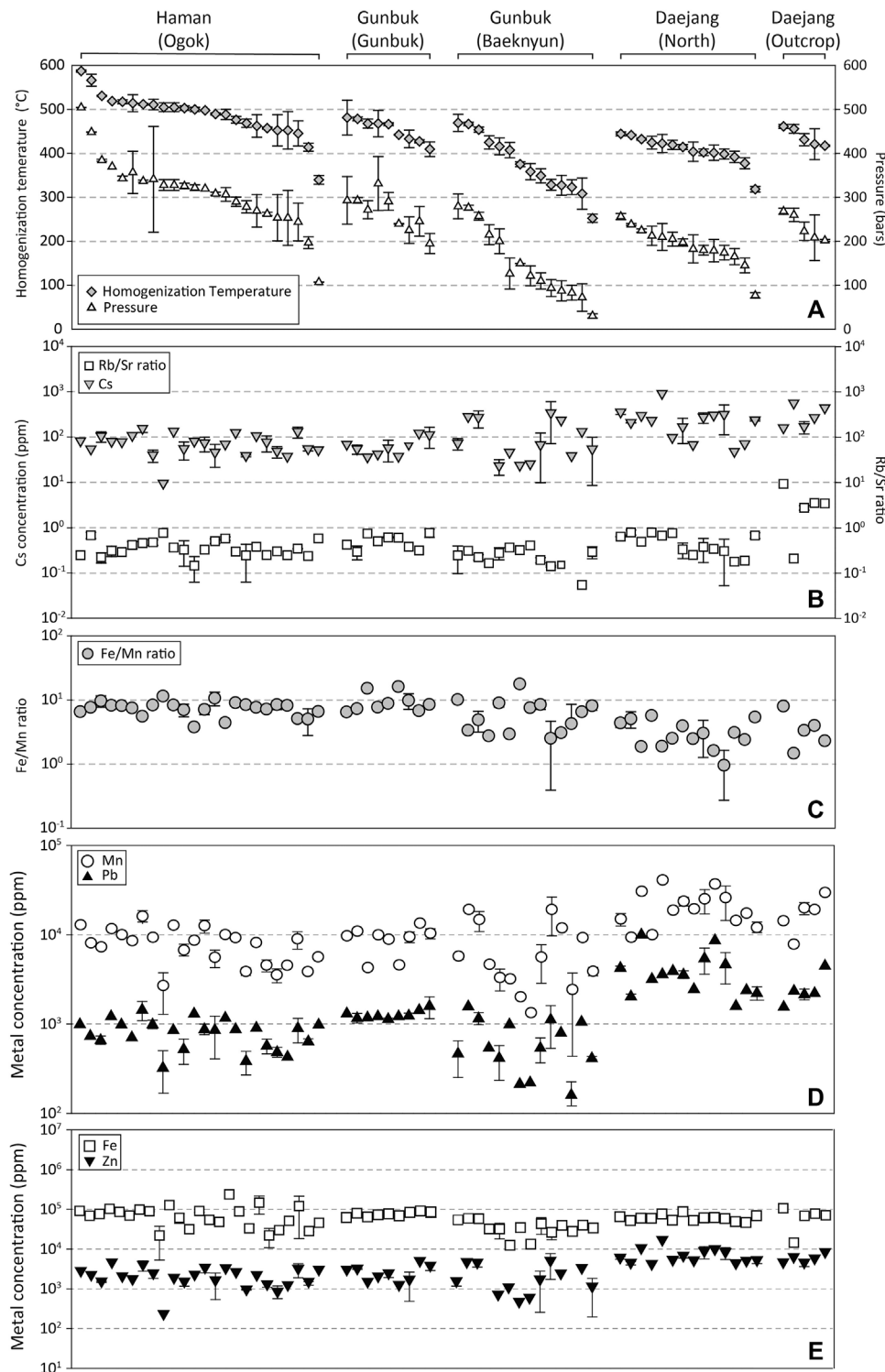


FIGURE 13 | Rb/Sr and Fe/Mn ratio, and concentrations of Cs, Mn, Pb, Fe, and Zn plotted in order of decreasing homogenization temperatures (T_h) of brine inclusion assemblages in orebodies of the Haman, Gunbuk, and Daejang deposits. **(A)** T_h and calculated P of brine inclusion assemblages. **(B)** Rb/Sr ratios and Cs concentrations of brine inclusion assemblages. Rb/Sr ratios and Cs concentrations in the Haman and Gunbuk deposits were lower than in the Daejang deposit. **(C)** Fe/Mn ratios were lower in the Daejang deposit than in the Haman and Gunbuk deposits. **(D)** Concentrations of Mn and Pb, and **(E)** Fe and Zn in brine inclusion assemblages. Mn, Pb, and Zn concentrations in the Daejang deposit were higher than in the Haman and Gunbuk deposits.

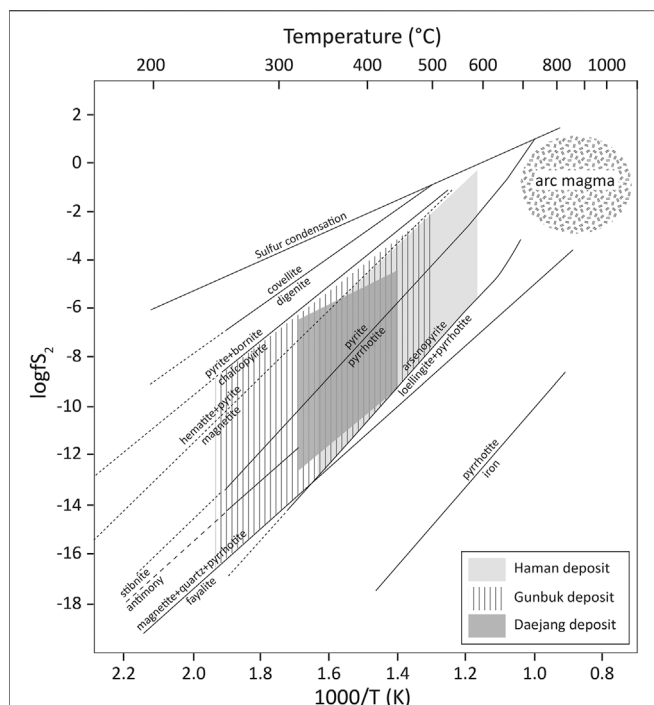


FIGURE 14 | The plot of hydrothermal temperatures versus sulfidation states of ore mineral assemblages, as described by Einaudi (2003) with some modification. Hydrothermal fluids of the Daejang deposit showed a higher sulfidation state (arsenopyrite-pyrrhotite-pyrite-chalcocopyrite, no magnetite) and a lower temperature range than the Haman and Gunbuk deposits (arsenopyrite-pyrrhotite-pyrite-chalcocopyrite, massive magnetite).

Giggenbach, 1993). Relative redox conditions in deposits can be compared using ratios of their Raman peak heights. The CO_2/CH_4 ratios of Raman peak heights from the Gunbuk and Daejang deposits were 4 and 9, respectively, which suggested more reducing fluid in the Gunbuk deposit. However, CO_2/CH_4 ratios measurements are limited by vapor inclusions, due to a possibility of post-entrapment ion or H_2 diffusion (Li et al., 2009; Zajacz et al., 2009; Seo and Heinrich, 2013) of fluid inclusions in quartz, which could modify gas ratios. The fluids in the three deposits were reduced more than those in typical porphyry-type deposits, comparisons of Fe/Mn ratios in brine inclusions and CO_2/CH_4 ratios in vapor inclusions in the three deposits suggested that fluids in the Daejang deposit were more oxidized than those in the Haman and Gunbuk deposits.

Since the three deposits are hosted within a shale formation (Figure 1), which is rich in organic carbon (Kim and Paik, 2001; Kim et al., 2018), differences between the redox states of fluids may have been caused by different degrees of interactions with the hosting shale. It was also noteworthy that, regardless of the redox conditions of the original magmatic ore fluids, fluid-rock interactions would effectively reduce fluids and precipitate ore minerals. Shale formation, therefore, in the study area might prove useful for exploring residual deposits.

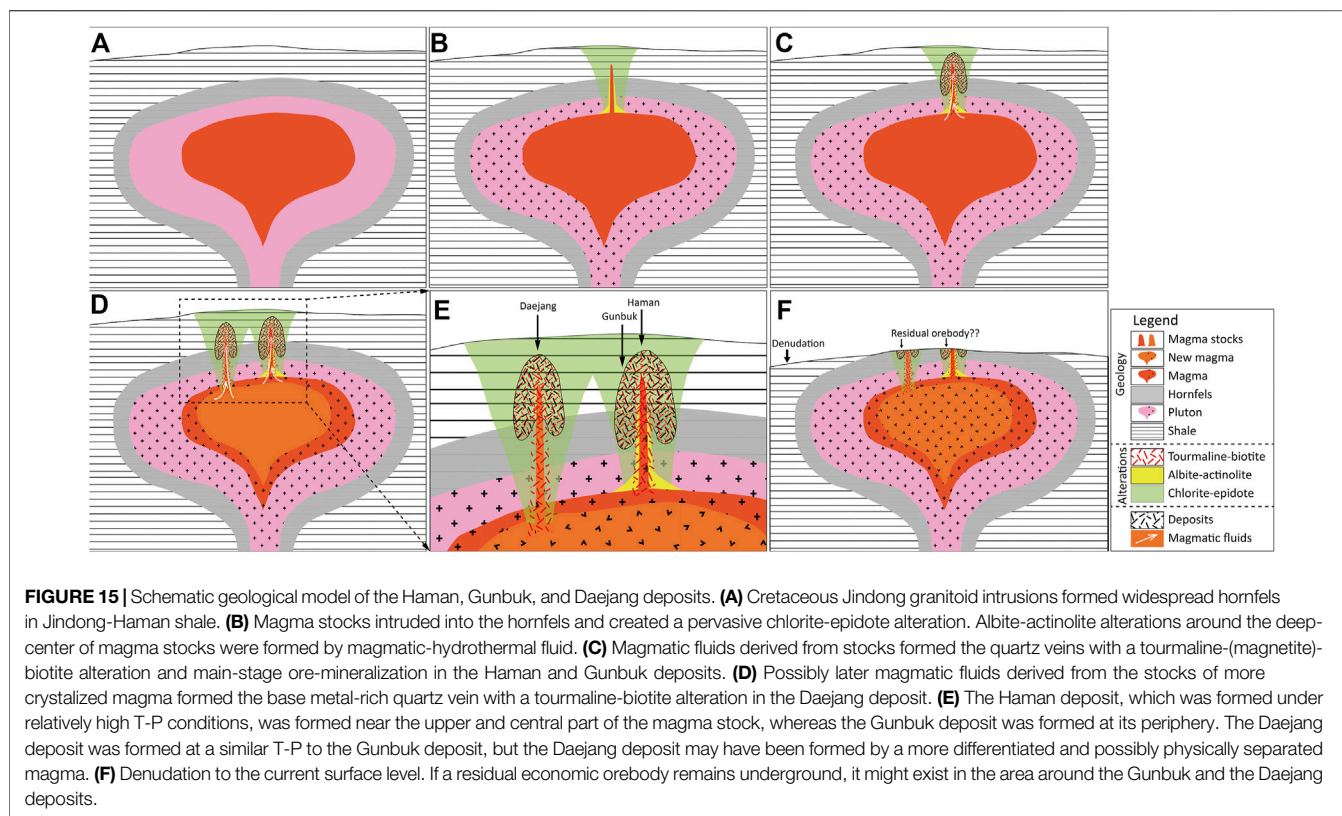
Rusk and Reed (2008) suggested hydrothermal fluid acidity controls Al concentrations in quartz, and thus, lower fluid pH

values, and that this is highly pronounced in quartz formed at lower temperatures ($<350^\circ\text{C}$) (Rusk and Reed, 2008). Similar Al concentrations in the quartz of Haman and Gunbuk deposits indicated similar pH conditions of ore-forming fluids (Figure 12A). The Ti content in quartz has been applied as a Ti-in-quartz geothermometer (Wark and Watson, 2006; Huang and Audétat, 2012) in TiO_2 saturated or rutile-bearing system. Although this geothermometer cannot be applied directly because the activities of TiO_2 in hydrothermal systems may not have achieved equilibrium (Huang and Audétat, 2012), temperature conditions can be compared. The maximum Ti concentration in the Haman deposit was higher than in the Gunbuk and Daejang deposits, which suggests a higher temperature in the Haman deposit and concurs with our microthermometry results (Figure 12B). If not in equilibrium, kinetically accumulated Al and Ti in hydrothermal quartz may represent the growth rate of the quartz in hydrothermal fluids (Müller et al., 2002; Huang and Audétat, 2012), which suggests higher growth rates of quartz veins in the Haman deposit than in the Daejang deposit (Figure 12).

The Rb/Sr ratios of magmatic-hydrothermal fluids are direct analogs of Rb/Sr ratios in causative magma. Since the Rb/Sr ratios in magma controlled by fractionation of K-feldspar and plagioclase, these ratios indicate a magma source or a degree of magma differentiation (Nockolds and Allen, 1953; Olade and Fletcher, 1975). Cs concentration in magmatic-hydrothermal fluids has been used to determine the fractionation degree of magma (Audétat and Pettke, 2003; Klemm et al., 2008; Lüders et al., 2009). The ranges of Rb/Sr ratios and Cs concentrations observed in brine inclusion assemblages (Figure 13B) suggest that magmatic-hydrothermal fluids that formed the Haman and Gunbuk deposits originated from magmas with similar degrees of differentiation, whereas those of the Daejang deposit indicate a more fractionated magma (Figure 13B). Relatively higher base metal (Zn and Pb) concentrations in the fluids of the Daejang deposit (Figures 13D,E) further support that this deposit may have been formed from a more differentiated magma than the Haman and Gunbuk deposits.

Geological Reconstruction of the Mineralization Processes

Concentrations of metals remain unchanged by changing the P-T conditions of fluids (Figures 13D,E), and the temperature ranges of ore-forming fluids are relatively higher than that required for copper mineralization ($<350^\circ\text{C}$) (Ayuso et al., 2010) in magmatic-hydrothermal deposits (Figure 9), indicating that a substantial ore at or below the current level of exposure may not be expected (Helgeson, 1969; Ulrich and Günther, 2001; Landtwing et al., 2005). Ore metals in the fluids might have precipitated above the current exposure, but we would expect that most of the economic portions of such deposits might have already been eroded, especially at the Haman deposit where high-temperature alteration minerals such as actinolite and hornblende prevail. The presence of a fluid inclusion



suggests that a deep (hydrostatically >5 km) hot (max. 600°C) magmatic-hydrothermal system exists in the Haman deposit that might be near the upper part of an intrusion center. However, the Gunbuk and Daejang deposits were formed shallower (hydrostatically <3 km) and under cooler conditions in Gunbuk and Daejang deposits (max. 500 and 460°C, respectively) than in the Haman deposit, possibly at the periphery or margin of intrusions.

The fluids in the Haman and Gunbuk deposits were derived from magma of similar level of differentiation, while the fluids in the Daejang deposit were derived from a rather fractionated or physically separated magma. Since the three deposits are neighboring and possibly interacted with an organic-rich shale formation, a varying degree of fluid-rock interaction with the shale could account for the different redox states of fluids in the area (i.e. Fe/Mn ratios in **Figure 13C**).

Geological models for the area can therefore be established. 1) The hornfels in the Haman-Jindong shale were formed around the pluton of late Cretaceous Jindong granitoids (**Figure 15A**). 2) A CE alteration in the hornfels was formed pervasively around the Jindong granitoids (**Figure 15B**). 3) External fluids (or magmatic fluids) formed the quartz veins accompanying the AA alteration (only in the Haman deposit) (**Figure 15B**). 4) Magmatic fluids formed the quartz veins accompanying TB alterations with Cu mineralization (**Figure 15C**). The Haman deposit was formed near the upper part of a sub-volcanic magma stock, while the Gunbuk deposit was formed shallower at the

periphery (**Figures 15D,E**). In the case of the Daejang deposit, magmatic-hydrothermal fluid is more differentiated than in the Haman-Gunbuk deposits. In the Daejang deposit, the ore precipitated shallower and at the periphery of magma (**Figures 15D,E**). The ore mineralogy in the Daejang deposit indicates a relatively higher sulfidation state than the magnetite-rich Haman and Gunbuk deposits. 5) The deposits were exposed to the current surface level by denudation, and a portion of economic orebodies appeared to have been substantially eroded (**Figure 15F**).

Comparison With Porphyry-Style Deposits and Exploration Potential in the Area

Rock-vein textures, alteration styles, and fluid inclusion types in the Haman, Gunbuk, and Daejang deposits were compared with the key characteristics of porphyry-style deposits. Geologic models of globally representative porphyry-style deposits, including an El Teniente Cu-Mo deposit (Klemm et al., 2007), Bingham Canyon Cu-Mo-Au deposit (Landtwing et al., 2005; Landtwing et al., 2010; Seo et al., 2012), and Ann Mason porphyry Cu deposit (Dilles and Einaudi, 1992), were applied to determine the possibility of a hidden economic ore in the studied area. The CE alteration in the study area corresponds to propylitic alteration of porphyry deposits. The CE alteration was pervasively distributed but only occurs in the hornfels of the Haman-Jindong shale. The CE alteration in hornfels can thus be used to vector the magmatic-hydrothermal or mineralization

center. Economic portions of porphyry deposits are typically associated with K-feldspar-biotite (potassic) and quartz-sericite (phyllic) alterations in deposits (Sillitoe, 2010). Main stage ore-bearing veins in the Haman, Gunbuk, and Daejang deposits are associated with the TB alteration (similar with the potassic alteration). Phyllic alteration was absent in studied deposits possibly because of large formation depths. Our fluid inclusion results show that the TB alteration in the studied deposits formed at a higher temperature than the temperature range of typical potassic alterations in porphyry deposits. T_h and pressure in brine inclusion assemblages in the El Teniente deposit are 320–410°C and max. 300 bar (Klemm et al., 2007), and about 350–410°C and max. 300 bar in the Bingham Canyon deposit (Landtwing et al., 2010). These P-T conditions are somewhat lower than those of the Haman deposit (340–600°C and max. 500 bar) but overlap with those of the Gunbuk (250–500°C and max. 330 bar) and Daejang deposits (320–460°C and max. 270 bar) (Figure 9A). The AA alteration that appears in the Haman deposit can be compared with the sodic-calcic alteration (Na-Ca alteration) of some porphyry deposits (Dilles and Einaudi, 1992; Sillitoe, 2010). P-T conditions and alteration styles suggest that the Haman deposit might represent a deep and barren part of a porphyry-style deposit. Although the maximum temperatures are generally higher than the range of porphyry deposits, the Gunbuk and Daejang deposits are closer to the “economic” temperature range. The alteration patterns and range of fluid temperatures observed suggest little possibility of an economic ore in the Haman deposit, but a possibility in the area of the Gunbuk and Daejang deposits. More studies of petrology and geochemistry such as on zircon fertility and stable isotopes in the area are required to fully understand its ore-forming processes and explore hidden economic orebodies.

CONCLUSION

Based on the petrography of the vein-bearing samples and the fluid inclusion studies conducted on Haman, Gunbuk, and Daejang deposits, we derive the following conclusions.

- 1) In the three deposits, pervasive CE alteration overprinting hornfels, TB alteration with ore mineralized quartz veins, and the latest barren calcite veins commonly occur.
- 2) The hydrothermal fluids of the Haman and Gunbuk deposits have relatively lower sulfidation and oxidation states than the Daejang deposit.
- 3) The Daejang deposit appears to have been formed from a relatively later differentiation stage magma than the Haman and Gunbuk deposits, which could result in distinctive ore mineral differences between the Daejang and Haman-Gunbuk deposits.
- 4) The Haman deposit was formed at the central-upper part of crystalizing magmatic stock under P-T conditions higher than

REFERENCES

Audétat, A., Gunther, D., and Heinrich, C. A. (1998). Formation of a Magmatic-Hydrothermal Ore deposit: Insights with LA-ICP-MS Analysis of Fluid Inclusions. *Science* 279, 2091–2094. doi:10.1126/science.279.5359.2091

those typical of economic porphyry Cu deposits. The Gunbuk and Daejang deposits were formed at a relatively shallow peripheral location and partially overlapped with the P-T conditions of porphyry deposits.

- 5) Because of the high fluid pressure and temperature, no large-scale Cu mineralization could be expected underneath the current exposure, especially in the Haman deposit. If there is an orebody remaining underneath, it might be placed in the vicinity of the Gunbuk and Daejang deposits.

DATA AVAILABILITY STATEMENT

The original contributions presented in the study are included in the article/**Supplementary Material**, further inquiries can be directed to the corresponding author.

AUTHOR CONTRIBUTIONS

TL and JS wrote the manuscript. TL, JS, BY, BL, and JL did fieldwork in the area. TL performed petrography of samples and fluid inclusion microthermometry. TL, JS, YY, and SH performed an LA-ICP-MS microanalysis. TL performed laser Raman spectroscopy. All authors discuss the results and correct the manuscript.

FUNDING

This work was supported by the National Research Council of Science and Technology (NST) grant by the Korean government (MSIT) (No. CRC-15-06-KIGAM) and the National Research Foundation (NRF) of Korea Grant funded by the Korea government (MSIT) (No. 2019R1C1C1002588). The LA-ICP-MS analysis was supported by KOPRI Research (PE 21050).

ACKNOWLEDGMENTS

The authors are indebted to professor Khin Zaw, professor Jung-Woo Park, and an reviewer for their constructive and insightful comments and reviews.

SUPPLEMENTARY MATERIAL

The Supplementary Material for this article can be found online at: <https://www.frontiersin.org/articles/10.3389/feart.2021.752908/full#supplementary-material>

Audétat, A., and Pettke, T. (2003). The magmatic-hydrothermal evolution of two barren granites: A melt and fluid inclusion study of the Rito del Medio and Canada Pinabete plutons in northern New Mexico (USA). *Geochimica et Cosmochimica Acta* 67 (1), 91–121. doi:10.1016/s0016-7037(02)01049-9

Ayuso, R. A., Barton, M. D., Blakely, R. J., Bodnar, R. J., Dilles, J. H., Gray, F., et al. (2010). “Porphyry Copper deposit Model: Chapter B of Mineral

- deposit Models for Resource Assessment,” in *U.S. Geological Survey Scientific Investigations Report 2010-5070-B*. Editor D. A. John (Virginia: U. S. Geological Survey).
- Barton, M. D., and Johnson, D. A. (1996). Evaporitic-source Model for Igneous-Related Fe Oxide-(ree-Cu-Au-U) Mineralization. *Geol* 24 (3), 2592. doi:10.1130/0091-7613(1996)024<0259:esmfr>2.3.co;2
- Barton, M. D., and Johnson, D. A. (2004). “Footprints of Fe-Oxide (-Cu-Au) Systems,” in *SEG 2004: Predictive Mineral Discovery Under Cover* Editors W. A. Perth, J. R. Muhling, and C. M. Knox-Robinson (Centre for Global Metallogeny, the University of Western Australia), 112–116.
- Boctor, N. Z. (1985). Rhodonite Solubility and Thermodynamic Properties of Aqueous $MnCl_2$ in the System $MnO-SiO_2-HCl-H_2O$. *Geochimica et Cosmochimica Acta* 49 (2), 565–575. doi:10.1016/0016-7037(85)90048-1
- Bodnar, R. J. (2003a). “Introduction to Fluid Inclusions,” in *Fluid Inclusions: Analysis and Interpretation*. Editors I. Samson, A. Anderson, and D. Marshall (Quebec City, Canada: Mineralogical Association of Canada Short Course), 1–8.
- Bodnar, R. J., and Vityk, M. O. (1994). “Interpretation of Microthermometric Data for $H_2O-NaCl$ Fluid Inclusions,” in *Fluid Inclusions in Minerals, Methods and Applications*. Editors B. D. Vivo and M. L. Frezzotti (Blacksburg, VA: Virginia Tech), 117–130.
- Bottrell, S. H., and Yardley, B. W. D. (1991). The Distribution of Fe and Mn between Chlorite and Fluid: Evidence from Fluid Inclusions. *Geochimica et Cosmochimica Acta* 55 (1), 241–244. doi:10.1016/0016-7037(91)90414-Z
- Carten, R. B. (1986). Sodium-calcium Metasomatism; Chemical, Temporal, and Spatial Relationships at the Yerington, Nevada, Porphyry Copper deposit. *Econ. Geology* 81 (6), 1495–1519. doi:10.2113/gsecongeo.81.6.1495
- Chang, K. H. (1977). Late Mesozoic Stratigraphy, Sedimentation and Tectonics of southeastern Korea. *J. Geol. Soc. Korea* 13, 76–90.
- Chang, K. H., Lee, Y. J., Suzuki, K., and Park, S. O. (1998). Zircon Morphology, CHIME Age and Geological Significance of Kusandong Tuff. *J. Geol. Soc. Korea* 34, 333–343.
- Choi, S.-G., Pak, S. J., Kim, C. S., Ryu, I.-C., and Wee, S.-M. (2006). The Origin and Evolution of Mineralizing Fluids in the Cretaceous Gyeongsang Basin, Southeastern Korea. *J. Geochemical Exploration* 89, 61–64. doi:10.1016/j.gexplo.2005.12.009
- Choi, S. H. (1998). Geochemical Evolution of Hydrothermal Fluids at the Daejang Cu-Zn-Pb Vein deposit, Korea. *Resource Geology* 48 (3), 171–182. doi:10.1111/j.1751-3928.1998.tb00015.x
- Choi, S. W. (1985). Fluid Inclusion Studies of the Haman-Gunbuk mMining District, Gyeongnam Province. *J. Educ. Res.* 17 (1), 123–146.
- Chough, S. K., and Sohn, Y. K. (2010). Tectonic and Sedimentary Evolution of a Cretaceous continental Arc-Backarc System in the Korean peninsula: New View. *Earth-Science Rev.* 101, 225–249. doi:10.1016/j.earscirev.2010.05.004
- Chough, S., Kwon, S.-T., Ree, J. H., and Choi, D. K. (2000). Tectonic and Sedimentary Evolution of the Korean Peninsula: A Review and New View. *Earth Sci. Rev.* 52, 175–235. doi:10.1016/s0012-8252(00)00029-5
- Chun, S. S., and Chough, S. K. (1992). “Tectonic History of Crataceous Sedimentary Basins in the Southwestern Korean Peninsula and Yellow Sea,” in *The Sedimentary Basins in the Korean Peninsula and Adjacent Seas*. Editor S. K. Chough (Hanlimwon, Seoul: Korean Sedimentology Research Group), 60–76.
- Dilles, J. H., Barton, M. D., Johnson, D. A., Proffett, J. M., Einaudi, M. T., and Crafford, E. J. (2000). “Part I. Contrasting Styles of Intrusion-Associated Hydrothermal Systems: Part II,” in *Geology & Gold Deposits of the Getchell Region* (Littleton, Colorado: Society of Economic Geologists).
- Dilles, J. H., and Einaudi, M. T. (1992). Wall-rock Alteration and Hydrothermal Flow Paths about the Ann-Mason Porphyry Copper deposit, Nevada; a 6-km Vertical Reconstruction. *Econ. Geology* 87 (8), 1963–2001. doi:10.2113/gsecongeo.87.8.1963
- Dreyer, B. M., Morris, J. D., and Gill, J. B. (2010). Incorporation of Subducted Slab-Derived Sediment and Fluid in Arc Magmas: B-Be-10Be- Nd Systematics of the Kurile Convergent Margin, Russia. *J. Petrol.* 51 (8), 1761–1782. doi:10.1093/ptetrology/eqq038
- Driesner, T., and Heinrich, C. A. (2007). The System $H_2O-NaCl$. Part I: Correlation Formulae for Phase Relations in Temperature-Pressure-Composition Space from 0 to 1000°C, 0 to 5000bar, and 0 to 1 XNaCl. *Geochimica et Cosmochimica Acta* 71 (20), 4880–4901. doi:10.1016/j.gca.2006.01.033
- Dubessy, J., Poty, B., and Ramboz, C. (1989). Advances in C-O-H-N-S Fluid Geochemistry Based on Micro-raman Spectrometric Analysis of Fluid Inclusions. *European Journal of Mineralogy* 1, 517–534. doi:10.1127/ejm/1/4/0517
- Einaudi, M. T., Hedenquist, J. W., and Inan, E. E. (2003). Sulfidation State of Fluids in Active and Extinct Hydrothermal Systems; Transitions from Porphyry to Epithermal Environments. *Soc. Econ. Geologists Spec. Publ.* 10, 285–313.
- Giggenbach, W. F. (1993). Redox Control of Gas Compositions in Philippine Volcanic-Hydrothermal Systems. *Geothermics* 22 (5), 575–587. doi:10.1016/0375-6505(93)90037-N
- Giggenbach, W. F. (1987). Redox Processes Governing the Chemistry of Fumarolic Gas Discharges from White Island, New Zealand. *Appl. Geochem.* 2 (2), 143–161. doi:10.1016/0883-2927(87)90030-8
- Goldstein, R. H., and Reynolds, T. J. (1994). Systematics of Fluid Inclusions in Diagenetic Minerals. *SEPM Soc. Sediment. Geology. Short Course*.
- Guillou, M., Meier, D., Allan, M. M., Heinrich, C. A., and Yardley, B. W. D. (2008). SILLS: a MATLAB-Based Program for the Reduction of Laser Ablation ICP-MS Data of Homogeneous Materials and Inclusions. *Mineralogical Assoc. Can. Short Course* 40, 328–333.
- Gustafson, L. B., and Hunt, J. P. (1975). The Porphyry Copper deposit at El Salvador, Chile. *Econ. Geology* 70 (5), 857–912. doi:10.2113/gsecongeo.70.5.857
- Heinrich, C. A., Günther, D., Audétat, A., Ulrich, T., and Frischknecht, R. (1999). Metal Fractionation between Magmatic Brine and Vapor, Determined by Microanalysis of Fluid Inclusions. *Geol* 27 (8), 755–758. doi:10.1130/0091-7613(1999)027<0755:mfbmba>2.3.co;2
- Heinrich, C. A., Pettko, T., Halter, W. E., Aigner-Torres, M., Audétat, A., Günther, D., et al. (2003). Quantitative Multi-Element Analysis of Minerals, Fluid and Melt Inclusions by Laser-Ablation Inductively-Coupled-Plasma Mass-Spectrometry. *Geochimica et Cosmochimica Acta* 67 (18), 3473–3497. doi:10.1016/S0016-7037(03)00084-X
- Helgeson, H. C. (1969). Thermodynamics of Hydrothermal Systems at Elevated Temperatures and Pressures. *Am. J. Sci.* 267 (7), 729–804. doi:10.2475/ajs.267.7.729
- Heo, C. H., Yun, S.-T., Choi, S. H., Choi, S.-G., and So, C.-S. (2003). Copper Mineralization in the Haman-Gunbuk Area, Gyeongsangnamdo-Province: Fluid Inclusion and Stable Isotope Study. *Econ. Environ. Geology* 36 (2), 75–87.
- Huang, R., and Audétat, A. (2012). The Titanium-In-Quartz (Titanium) Thermobarometer: a Critical Examination and Re-calibration. *Geochimica et Cosmochimica Acta* 84, 75–89. doi:10.1016/j.gca.2012.01.009
- Jin, M. S., Lee, S. M., Lee, J. S., and Kim, S. J. (1982). Litho-geochemistry of the Cretaceous Granitoids with Relation to the Metallic Ore Deposits in Southern Korea. *J. Geol. Soc. Korea* 18 (3), 119–131.
- Kim, H. J., Paik, I. S., Kim, S., and Lee, H. (2018). Sedimentary Facies, Paleoenvironments, and Stratigraphy of the Haman Formation (Early Cretaceous) in Sopo-Ri, Haman-Gun, Gyeongsangnam-Do, Korea. *Jgsk* 54 (1), 1–19. doi:10.14770/jgsk.2018.54.1.1
- Kim, H. J., and Paik, I. S. (2001). Sedimentary Facies and Environments of the Cretaceous Jindong Formation in Goseong-Gun, Gyeongsangnamdo. *J. Geol. Soc. Korea* 37 (2), 235–256.
- Kim, N., Koh, S.-M., You, B.-W., and Lee, B. H. (2021). Mineralogy, Geochemistry, and Age Constraints on the Axinite-Bearing Gukjeon Pb-Zn Skarn Deposit in the Miryang Area, South Korea. *Minerals* 11 (6), 619. doi:10.3390/min11060619
- Kim, O. J., and Kim, K. H. (1974). A Study on Red Hill Copper Deposits of the Dongjom Mine. *J. Korean Inst. Mining Geology* 7 (4), 157–174. doi:10.4097/kjae.1974.7.1.145
- Kim, S. U. (1973). A Regional Study for Developments of Kyeongnam Copper Metallogenic Province. *J. Korean Inst. Mining Geology* 6 (3), 133–170. doi:10.4097/kjae.1973.6.2.247
- Kim, S. W., Kwon, S., Park, S.-I., Lee, C., Cho, D.-L., Lee, H.-J., et al. (2016a). SHRIMP U-Pb Dating and Geochemistry of the Cretaceous Plutonic Rocks in the Korean Peninsula: A New Tectonic Model of the Cretaceous Korean Peninsula. *Lithos* 262, 88–106. doi:10.1016/j.lithos.2016.06.027
- Kim, Y. H., Hwang, H. G., Baek, G., Seo, J. R., Choi, D. H., Kang, J. N., et al. (2016b). Uiryeong District (Cu) Detailed Investigation Report. *Uiryeong* 117, 127.
- Klemm, L. M., Pettko, T., Heinrich, C. A., and Campos, E. (2007). Hydrothermal Evolution of the El Teniente Deposit, Chile: Porphyry Cu-Mo Ore Deposition from Low-Salinity Magmatic Fluids. *Econ. Geology* 102 (6), 1021–1045. doi:10.2113/gsecongeo.102.6.1021

- Klemm, L. M., Pettke, T., and Heinrich, C. A. (2008). Fluid and Source Magma Evolution of the Questa Porphyry Mo deposit, New Mexico, USA. *Miner Deposita* 43 (5), 533–552. doi:10.1007/s00126-008-0181-7
- Koh, S.-M., Ryou, C.-R., and Song, M.-S. (2003). Mineralization Characteristics and Structural Controls of Hydrothermal Deposits in the Gyeongsang Basin, South Korea. *Resource Geology*. 53 (3), 175–192. doi:10.1111/j.1751-3928.2003.tb00168.x
- Kooiman, G. J. A., McLeod, M. J., and Sinclair, W. D. (1986). Porphyry Tungsten-Molybdenum Orebodies, Polymetallic Veins and Replacement Bodies, and Tin-Bearing Greisen Zones in the Fire Tower Zone, Mount Pleasant, New Brunswick. *Econ. Geology*. 81 (6), 1356–1373. doi:10.2113/gsecongeo.81.6.1356
- Landtwing, M., Pettke, T., Halter, W., Heinrich, C., Redmond, P., Einaudi, M., et al. (2005). Copper Deposition during Quartz Dissolution by Cooling Magmatic-Hydrothermal Fluids: The Bingham Porphyry. *Earth Planet. Sci. Lett.* 235 (1), 229–243. doi:10.1016/j.epsl.2005.02.046
- Landtwing, M. R., Furrer, C., Redmond, P. B., Pettke, T., Guillong, M., and Heinrich, C. A. (2010). The Bingham Canyon Porphyry Cu-Mo-Au Deposit. III. Zoned Copper-Gold Ore Deposition by Magmatic Vapor Expansion. *Econ. Geology*. 105, 91–118. doi:10.2113/gsecongeo.105.1.91
- Lee, H. K., and Moon, H.-S. (1989). Ore Minerals and the Physicochemical Environments of the Inseong Gold-Silver Deposits, Republic of Korea. *J. Korean Inst. Mining Geology*. 22 (3), 237–252.
- Lee, J. K., and Lee, J. Y. (1994). Trace Elements Geochemistry and Copper Mineralization of Jindong Granitic Rocks. *J. Geol. Soc. Korea* 30 (5), 455–466.
- Lee, J. Y. (1989). A Geochemical Study on the Chindong and Yucheon-Eonyang Granites in Relation to Mineralization. *J. Korean Inst. Mining Geology*. 22 (1), 21–34.
- Lee, J. Y., Lee, J. K., Par, B. J., Lee, I. H., and Kim, S. W. (1994). A Geochemical Study on Jindong Granites in Relation to Copper Ore Deposits in Gyeongsang basin. *Econ. Environ. Geology*. 27 (2), 161–170.
- Lee, S. Y., Choi, S.-G., So, C. H., Ryu, I. C., Wee, S. M., and Heo, C. H. (2003). Basemental Mineralization in the Cretaceous Gyeongsang Basin and its Genetic Implications, Korea : the Haman-Gunbug-Goseong(-Changwon) Amd the Euseong Metallogenic Provinces. *Econ. Environ. Geology*. 36 (4), 257–268.
- Leeman, W. P., Carr, M. J., and Morris, J. D. (1994). Boron Geochemistry of the Central American Volcanic Arc: Constraints on the Genesis of Subduction-Related Magmas. *Geochimica et Cosmochimica Acta* 58 (1), 149–168. doi:10.1016/0016-7037(94)90453-7
- Li, Y., Audétat, A., Lerchbaumer, L., and Xiong, X. L. (2009). Rapid Na, Cu Exchange between Synthetic Fluid Inclusions and External Aqueous Solutions: Evidence from LA-ICP-MS Analysis. *Geofluids* 9 (4), 321–329. doi:10.1111/j.1468-8123.2009.00255.x
- Lüders, V., Romer, R. L., Gilg, H. A., Bodnar, R. J., Pettke, T., and Misantoni, D. (2009). A Geochemical Study of the Sweet Home Mine, Colorado Mineral Belt, USA: Hydrothermal Fluid Evolution above a Hypothesized Granite Cupola. *Miner Deposita* 44, 415–434. doi:10.1007/s00126-008-0221-3
- Lynch, G., and Ortega, J. (1997). Hydrothermal Alteration and Tourmaline-Albite Equilibria at the Coxheath Porphyry Cu-Mo-Au deposit, Nova Scotia. *Can. Mineral.* 35 (1), 79–94.
- Mark, G., and Foster, D. R. W. (2000). Magmatic-hydrothermal Albite-Actinolite-Apatite-Rich Rocks from the Cloncurry District, NW Queensland, Australia. *Lithos* 51, 223–245. doi:10.1016/s0024-4937(99)00069-9
- Min, K. D., Kim, O. J., Yun, S. K., Lee, D. S., and Joo, S. W. (1982). Applicability of Plate Tectonics to the post-late Cretaceous Igneous Activities and Mineralization in the Southern Part of South Korea(I). *J. Korean Inst. Mining Geology*. 15 (3), 123–154.
- Moon, C. U., Kim, M. W., Lee, J. H., and Chai, C. J. (1986). *Geological Investigation Report of Copper Deposits on the Haman-Gunbuk District*. Wonju, South Korea: Korea resources corporation.
- Moon, C. U., Kim, M. W., Lee, J. H., and Choi, C. J. (1970). Geology and Ore Deposits in Haman-Kunbuk Copper Deposit. *J. Korean Inst. Mining Geology*. 3 (2), 55–73.
- Moran, A. E., Sisson, V. B., and Leeman, W. P. (1992). Boron Depletion during Progressive Metamorphism: Implications for Subduction Processes. *Earth Planet. Sci. Lett.* 111 (2), 331–349. doi:10.1016/0012-821X(92)90188-2
- Müller, A., Kronz, A., and Breiter, K. (2002). Trace Elements and Growth Patterns in Quartz: a Fingerprint of the Evolution of the Subvolcanic Podlesi Granite System (Krusné Hory Mts., Czech Republic). *Bull. Geosciences* 77 (2), 135–145.
- Naeher, S., Gilli, A., North, R. P., Hamann, Y., and Schubert, C. J. (2013). Tracing Bottom Water Oxygenation with Sedimentary Mn/Fe Ratios in Lake Zurich, Switzerland. *Chem. Geology*. 352, 125–133. doi:10.1016/j.chemgeo.2013.06.006
- Nockolds, S. R., and Allen, R. (1953). The Geochemistry of Some Igneous Rock Series. *Geochimica et Cosmochimica Acta* 4, 105–142. doi:10.1016/0016-7037(53)90055-6
- Olade, M. A., and Fletcher, W. K. (1975). Primary Dispersion of Rubidium and Strontium Around Porphyry Copper Deposits, Highland Valley, British Columbia. *Econ. Geology*. 70, 15–21. doi:10.2113/gsecongeo.70.1.15
- Oliver, N. H. S. (1996). Review and Classification of Structural Controls on Fluid Flow during Regional Metamorphism. *J. Metamorph Geol.* 14 (4), 477–492. doi:10.1046/j.1525-1314.1996.00347.x
- Orován, E. A., Cooke, D. R., Harris, A. C., Ackerman, B., and Lawlis, E. (2018). Geology and Isotope Geochemistry of the Wainaulo Cu-Au Porphyry Deposit, Namosi District, Fiji. *Econ. Geology*. 113 (1), 133–161. doi:10.5382/econgeo.2018.4546
- Pacey, A., Wilkinson, J. J., and Cooke, D. R. (2020). Chlorite and Epidote Mineral Chemistry in Porphyry Ore Systems: A Case Study of the Northparkes District, New South Wales, Australia. *Econ. Geology*. 115 (4), 701–727. doi:10.5382/econgeo.4700
- Park, H. I., Choi, S.-W., Chang, H. W., and Chae, D. H. (1985). Copper Mineralization at Haman-Gunbuk Mining District, Gyeongnam Area. *J. Korean Inst. Mining Geology*. 18 (2), 107–124.
- Park, H. I., Choi, S. W., Chang, H. W., and Lee, M. S. (1983). Genesis of the Copper Deposits in Goseong District, Gyeongnam Area. *J. Korean Inst. Mining Geology*. 16 (3), 135–147. doi:10.4070/kcj.1983.13.1.135
- Park, H. I., and Kim, D. L. (1988). The Mode of Occurrence and Depositional Conditions of Antimony Minerals from North Ore Deposits of the Daejang Mine. *J. Geol. Soc. Korea* 24 (3), 251–266.
- Park, H. I., and Seol, Y. K. (1992). The Copper Mineralization of the Keumryeong and Kigu Ore Deposits. *J. Korean Inst. Mining Geology*. 25 (3), 283–296.
- Perring, C. S., Pollard, P. J., Dong, G., Nunn, A. J., and Blake, K. L. (2000). The Lightning Creek Sill Complex, Cloncurry District, Northwest Queensland: A Source of Fluids for Fe Oxide Cu-Au Mineralization and Sodic-Calcic Alteration. *Econ. Geology*. 95 (5), 1067–1089. doi:10.2113/gsecongeo.95.5.1067
- Pollard, P. J., Blake, K. L., and Dong, G. (1997a). “Proterozoic Cu-Au-Co and Pb-Zn-Ag Mineralization in the Cloncurry District, Eastern Mount Isa Inlier, Australia: Constraints on Fluid Sources from Mineralogical, Fluid Inclusion and Stable Isotope Data,” in *Final Report of AMIRA P438*. Editor P. J. Pollard (Cloncurry: Cloncurry base metals and gold).
- Reed, M. H., and Palandri, J. (2006). 11. Sulfide Mineral Precipitation from Hydrothermal Fluids. *Rev. Mineralogy Geochem.* 61 (1), 609–632. doi:10.1515/9781501509490-012
- Roedder, E., and Bodnar, R. J. (1980). Geologic Pressure Determinations from Fluid Inclusion Studies. *Annu. Rev. Earth Planet. Sci.* 8, 263–301. doi:10.1146/annurev.ea.08.050180.001403
- Rusk, B. G., Lowers, H. A., and Reed, M. H. (2008). Trace Elements in Hydrothermal Quartz: Relationships to Cathodoluminescent Textures and Insights into Vein Formation. *Geol* 36 (7), 547–550. doi:10.1130/g24580a.1
- Ryu, I. C., Choi, S.-G., and Wee, S. M. (2006). An Inquiry into the Formation and Deformation of the Cretaceous Gyeongsang (Kyeongsang) Basin, Southeastern Korea. *Econ. Environ. Geology*. 39 (2), 129–149.
- Seedorf, E., Dilles, J. H., Proffett, J. M., Jr., Einaudi, M. T., Zurcher, L., Stavast, W. J. A., et al. (2005). “Porphyry Deposits: Characteristics and Origin of Hypogene Features,” in *One Hundredth Anniversary Volume* (Littleton, Colorado: Society of Economic Geologists).
- Seo, J. H., Guillong, M., and Heinrich, C. A. (2012). Separation of Molybdenum and Copper in Porphyry Deposits: The Roles of Sulfur, Redox, and pH in Ore mineral Deposition at Bingham Canyon. *Econ. Geology*. 107, 333–356. doi:10.2113/econgeo.107.2.333
- Seo, J. H., and Heinrich, C. A. (2013). Selective Copper Diffusion into Quartz-Hosted Vapor Inclusions: Evidence from Other Host Minerals, Driving Forces, and Consequences for Cu-Au Ore Formation. *Geochimica et Cosmochimica Acta* 113, 60–69. doi:10.1016/j.gca.2013.03.016
- Seo, M. (2016). *Cu Mineralization of the Ilkwang Breccia Pipe-type Copper Deposit*. Busan: Master, Pusan National University.
- Shin, H. J., Kim, M. Y., and So, C.-S. (1987). Geochemistry and Genetic Environments of the Daejang Vein Deposits. *J. Korean Inst. Mining Geology*. 20 (1), 61–75. doi:10.4097/kjge.1987.20.5.707

- Sillitoe, R. H. (1980). Evidence for Porphyry-type Mineralization in Southern Korea. *Mining Geology. Spec. Issue.* 8, 205–214. doi:10.1130/0091-7613(1980)8<11:apcakm>2.0.co;2
- Sillitoe, R. H. (2010). Porphyry Copper Systems. *Econ. Geology.* 105, 3–41. doi:10.2113/gsecongeo.105.1.3
- Sillitoe, R. H., and Sawkins, F. J. (1971). Geologic, Mineralogic and Fluid Inclusion Studies Relating to the Origin of Copper-Bearing Tourmaline Breccia Pipes, Chile. *Econ. Geology.* 66 (7), 1028–1041. doi:10.2113/gsecongeo.66.7.1028
- Sinclair, W. (2007). *Porphyry Deposits*, 223–243.
- So, C.-S., Chi, S.-J., Shelton, K. L., and Skinner, B. J. (1985). Copper-bearing Hydrothermal Vein Deposits in the Gyeongsang Basin, Republic of Korea. *Econ. Geology.* 80 (1), 43–56. doi:10.2113/gsecongeo.80.1.43
- So, C.-S., Choi, S.-H., and Yun, S.-T. (1995). Geochemistry and Genesis of Hydrothermal Cu Deposits in the Gyeongsang Basin, Korea: Hwacheon-Ri Mineralized Area. *Econ. Environ. Geology.* 28 (4), 337–350.
- Uchida, E., Choi, S.-G., Baba, D., and Wakisaka, Y. (2012). Petrogenesis and Solidification Depth of the Jurassic Daebo and Cretaceous Bulguksa Granitic Rocks in South Korea. *Resource Geology.* 62 (3), 281–295. doi:10.1111/j.1751-3928.2012.00195.x
- Ulrich, T., Gunther, D., and Heinrich, C. A. (2001). The Evolution of a Porphyry Cu-Au Deposit, Based on LA-ICP-MS Analysis of Fluid Inclusions: Bajo de la Alumbrera, Argentina. *Econ. Geology.* 96, 1743–1774. doi:10.2113/gsecongeo.96.8.1743
- Wark, D. A., and Watson, E. B. (2006). TitaniQ: a Titanium-In-Quartz Geothermometer. *Contrib. Mineral. Petrol.* 152 (6), 743–754. doi:10.1007/s00410-006-0132-1
- Wee, S. M., Kim, Y.-J., Choi, S.-G., Park, J. W., and Ryu, I. C. (2007). Adakitic Signatures of the Jindong Granitoids. *Econ. Environ. Geology.* 40 (2), 223–236.
- Wilkinson, J. J., Baker, M. J., Cooke, D. R., and Wilkinson, C. C. (2020). Exploration Targeting in Porphyry Cu Systems Using Propylitic Mineral Chemistry: A Case Study of the El Teniente Deposit, Chile. *Econ. Geology.* 115 (4), 771–791. doi:10.5382/econgeo.4738
- Williams, P. J., Barton, M. D., Johnson, D. A., Fontbote, L., de Haller, A., Mark, G., et al. (2005). “Iron Oxide Copper-Gold Deposits; Geology, Space-Time Distribution, and Possible Modes of Origin,” in *Economic Geology 100th Anniversary Volume*. Editors J. W. Hedenquist, J. F. H. Thompson, R. J. Goldfarb, and J. P. Richards (Littleton CO: Society of Economic Geologists), 371–405.
- Won, J. G., and Kim, K. T. (1966). On the Geology and Mineralization in Dalsung Mine Area. *J. Geol. Soc. Korea* 2 (1), 52–69.
- Xavier, R. P., Wiedenbeck, M., Trumbull, R. B., Dreher, A. M., Monteiro, L. V. S., Rhede, D., et al. (2008). Tourmaline B-Isotopes Fingerprint marine Evaporites as the Source of High-Salinity Ore Fluids in Iron Oxide Copper-Gold Deposits, Carajás Mineral Province (Brazil). *Geol* 36 (9), 743–746. doi:10.1130/g24841a.1
- Yang, K. H., and Jang, J.-Y. (2002). Geochemistry of Tourmaline in the Ilhwang Cu-W Breccia-Pipe deposit, Southeastern Gyeongsang Basin. *J. Petrological Soc. Korea* 11 (3-4), 259–270.
- Zajacz, Z., Hanley, J. J., Heinrich, C. A., Halter, W. E., and Guillong, M. (2009). Diffusive Reequilibration of Quartz-Hosted Silicate Melt and Fluid Inclusions: Are All Metal Concentrations Unmodified? *Geochimica et Cosmochimica Acta* 73 (10), 3013–3027. doi:10.1016/j.gca.2009.02.023

Conflict of Interest: The authors declare that the research was conducted in the absence of any commercial or financial relationships that could be construed as a potential conflict of interest.

Publisher’s Note: All claims expressed in this article are solely those of the authors and do not necessarily represent those of their affiliated organizations, or those of the publisher, the editors and the reviewers. Any product that may be evaluated in this article, or claim that may be made by its manufacturer, is not guaranteed or endorsed by the publisher.

Copyright © 2021 Lee, Seo, Yoo, Lee, Han, Yang and Lee. This is an open-access article distributed under the terms of the Creative Commons Attribution License (CC BY). The use, distribution or reproduction in other forums is permitted, provided the original author(s) and the copyright owner(s) are credited and that the original publication in this journal is cited, in accordance with accepted academic practice. No use, distribution or reproduction is permitted which does not comply with these terms.